[redacted]

[redacted]

Copy 196
RM L55J28

NACA RM L55J28

TECH LIBRARY KAFB, NM
0143558

NACA

Reg # 10021

RESEARCH MEMORANDUM

7660

ANALYSIS OF A FLIGHT INVESTIGATION AT SUPERSONIC SPEEDS OF A SIMPLE HOMING SYSTEM

By Robert A. Gardiner, Clarence L. Gillis,
and G. B. Graves, Jr.

Langley Aeronautical Laboratory
Langley Field, Va.

HADC
TECHNICAL LIBRARY
AFL 2811

[redacted]

NATIONAL ADVISORY COMMITTEE
FOR AERONAUTICS
WASHINGTON
January 10, 1956

[redacted]

[redacted]

Classification cancelled (or changed to UNCLASSIFIED)

By Authority of NASA TECH PUB ANNOUNCEMENT #124
(OFFICER AUTHORIZED TO CHANGE)

By 10 FEB 58
NAME AND

GRADE OF OFFICER MAKING CHANGE)

28 Mar 61
DATE

1G

TECH LIBRARY KAFB, NM
0143558

NATIONAL ADVISORY COMMITTEE FOR AERONAUTICS

RESEARCH MEMORANDUM

ANALYSIS OF A FLIGHT INVESTIGATION AT SUPERSONIC SPEEDS OF A SIMPLE HOMING SYSTEM

By Robert A. Gardiner, Clarence L. Gillis,
and G. B. Graves, Jr.

SUMMARY

A flight investigation of a simple homing device utilizing unique guidance principles has been conducted. From the telemetered data and the photographic records of the trajectory of a supersonic test missile homing on a parachute flare, it is concluded that the principle of guidance and control exemplified by the simple homing system is fundamentally sound. As a result of analog studies concerned primarily with the ratio of rolling frequency to airframe frequency, it is concluded that considerable system improvement may be obtained from further research.

INTRODUCTION

A simple homing device has been proposed to reduce the dispersion of rockets used for armament of high-speed interceptor aircraft. The intention was to reduce the accuracy required from the airborne fire control system as well as to reduce dispersion. The basic idea involves using some of the aerodynamic capabilities of the airframe to replace some of the normal homing system functions.

The principles of operation of the device and results of simulator studies have been described in detail in references 1 and 2.

The purpose of the flight investigation described herein was as a "proof" check of the system and to determine what effect several variables which could not be practicably simulated would have on the operation.

A team of research scientists at the Langley Aeronautical Laboratory was assigned to carry out this project. The authors are particularly indebted to the following for their special contributions as members of this team:

[redacted]

Clarence A. Brown, Jr., Pilotless Aircraft Research Division
H. Douglas Garner, Instrument Research Division
Anthony L. Passera, Pilotless Aircraft Research Division
Henry J. E. Reid, Jr., Instrument Research Division

OPERATING PRINCIPLES

If pursuit (or chase) type of navigation is used in a homing system, it is possible to require only two types of flight from the airframe. If the missile velocity and sight line are alined, the airframe must fly straight. If an error exists between the line of sight to the target and the velocity, the flight path must be curved in a direction to reduce the error. In this system these two types of operation are obtained by control of the roll orientation.

The airframe is operated with fixed incidence elevators. Thus lift is always being produced. If the airframe is rolled continuously, a helix will be generated; but the direction of flight will be essentially straight. If the roll angle is controlled so as to point the lift in the direction of the error between line of sight and missile velocity, the flight path will be curved in a direction to reduce the error.

The type of roll control used in this system was chosen so that only full aileron deflection was required to generate the two modes of operation of the airframe. On-off control, where the reversal of the corrective rolling moment is required when the airframe lift vector crosses the missile-target line of sight, was used to control roll orientation. This type of roll control acts to cause hunting in roll on the target. This mode of operation oriented the lift vector approximately in the direction of flight path error and produced a curved corrective flight path. When the flight path error was reduced to a small value (also before target acquisition), the airframe rolled continuously and flew on a straight flight path.

The seeker used with this system must be capable of detecting targets within a narrow rectangle. The elements of this detecting system are boresighted with the missile axis in such a manner as to aline one end of the detecting rectangle with the axis around which the missile rolls, while the other end is alined in the direction of lift, as shown in figure 1.

In operation the airframe and seeker function together as follows: when the missile rolls, the seeker scans a 12° included angle cone with about a 2° central dead zone. Figure 2 illustrates this operation. If a target is located within the active area of this cone, as the missile rolls the detecting area will cross the target and produce a signal.

This signal is used to reverse the ailerons causing roll in the opposite direction. This causes the detecting area to recross the target and again reverse the ailerons. Thus, the missile hunts in roll on the target.

As the missile hunts, the flight path of the missile is curved toward the target, since the detecting area and the lift of the airframe are alined to produce this direction of flight-path correction. As the flight path curves, the relative motion between missile and target causes the target to appear to move toward the center end of the seeker rectangle. When the missile is pointed directly toward the target, the target moves into the central dead spot of the seeker, the roll control is inactive, and the missile rolls continually while moving toward the target on an effective straight flight path.

SYMBOLS

C_D	total drag coefficient, $\frac{\text{Drag}}{qS}$
C_N	total normal force coefficient, $\frac{\text{Normal force}}{qS}$
C_L	total lift coefficient, $\frac{\text{Lift}}{qS}$
C_L'	lift coefficient of nose section including canard surfaces
C_m	pitching-moment coefficient, $\frac{\text{Pitching moment}}{qSd}$
C_l	rolling-moment coefficient, $\frac{\text{Rolling moment}}{qSd}$
l	rolling moment
p	rolling angular velocity, radians per sec
a	resultant acceleration normal to longitudinal axis, as measured by accelerometers, g units
d	diameter of nose section, 0.458 ft
M	Mach number
M_o	initial (launching) Mach number

S	cross-sectional area of nose section, 0.165 sq ft
t	time from launching, sec
q	dynamic pressure, lb/sq ft
$\phi_f - a$	relative roll angle between forward and aft end of missile, deg
α	angle of attack, deg
I_Y	moment of inertia of entire model in pitch, slug-ft^2
I_X	moment of inertia of entire model in roll, slug-ft^2
I_X'	moment of inertia in roll of section forward of roll bearing, slug-ft^2
δ_c	deflection of pitch canard surface, deg
δ_f	deflection of lift-cancellation flap, deg, measured with respect to canard surface chord line
δ_a	deflection of each aileron, deg
δ_v	deflection of vertical canard surfaces, deg
ω	circular frequency, radians per sec

A symbol used as a subscript represents the partial derivative of a quantity with respect to the subscript; for example, $C_{L_{\delta_c}}' = \frac{\partial C_L'}{\partial \delta_c}$

MODEL AND AERODYNAMIC DESIGN

Model Description

A sketch of the model configuration used in the flight test described herein is shown in figure 3, and photographs are presented in figure 4. The model consists of a standard HPAG rocket with a set of cruciform wings of 60° delta plan form mounted on the rear end; and a forward section containing the seeker, pneumatic control system, cruciform canard fins, telemeter, and accelerometers, mounted on the forward end of the rocket.

A conical windshield, supported by an octapod is mounted ahead of the flat nose (fig. 4(b)). The roll bearing in the forward section (fig. 3(b)) permits freedom in roll between the part of the model ahead of, and the part behind the bearing. Dimensions of the control surfaces are shown in figure 3(c). The two surfaces which are alined with the seeker-detecting element contain partial-span trailing-edge ailerons for roll control (fig. 4(c)). The two surfaces at right angles to the first two provide pitch control; and these surfaces along with their trailing-edge flaps are set at fixed deflections (figure 4(d)). All of this forward section of the model is simply screwed onto the head cap of the HPAG rocket and requires no other connection to the rear end. Dimensions of the wings are given in figure 3(c). Two launching lugs are strapped to the rocket case as shown. Flares are fastened to two of the wing tips (fig. 4(d)) to furnish a light source for photographic tracking of the model during the after-dark flight test.

During the course of the development of the configuration some changes were required, as will be explained in detail later. Some of the data contained herein were obtained with the earlier configuration (see fig. 5), which differed from the configuration shown in figure 3 in the following ways:

(1) The windshield, ahead of the nose, was mounted on a tripod instead of an octapod.

(2) The corner at the nose was left sharp rather than rounded.

(3) The control surfaces were of 60° delta plan form; two all-movable surfaces were used for roll control, and the other two (without trailing-edge flaps) were set at a fixed deflection for pitch control.

(4) The roll bearing section was shorter and of different internal arrangement. The redesign was required to minimize friction.

The mass characteristics and nominal control-surface deflections used in the flight investigation described herein are given in the following tables:

Mass Characteristics

	Rocket loaded	Rocket empty
Weight, lb	149.0	104.0
I_Y, slug-ft^2	39.5	32.0
I_X, slug-ft^2	0.22	0.18
I_X', slug-ft^2	0.04	0.04
Center of gravity, in. from station 0	78.8	70.0

Control-Surface Deflection

δ_a, deg	±5.1
δ_c, deg	+3.7
δ_f, deg	-6.9
δ_v, deg	0

Choice of Configuration

Because of the exploratory nature of this project the specifications covering the airframe aerodynamic design were not particularly comprehensive or exacting. In order not to depart too far from practicality, however, the following objectives were kept in mind and were influential in determining the configuration:

(1) Use of standard components and parts where possible.

(2) Simplicity in the operation of the system and in its operational use.

(3) Air-to-air operation against aircraft with speeds in the region of Mach number 1.0 and altitudes up to 50,000 feet.

(4) Initial experimental phase to employ ground launching, but model to be suitable for air launching with no major changes.

(5) Development cost and tests to be kept to a minimum.

The method of operation, described previously, in which the searching and homing phases of flight were accomplished by controlling the roll, could be accomplished by rolling the entire missile or only part of it. The latter scheme with only the missile forward end controlled in roll was selected since it had several important advantages: the roll inertia was reduced; the required control-surface size and control-system power requirements were reduced; induced aerodynamic rolling moments on the rear lifting surfaces did not affect the roll control; and placing all the operating mechanism in the forward end simplified the design, construction, and operational use of the vehicle.

To avoid the necessity of specially ground lenses and to minimize optical difficulties, the window for the seeker was composed of a piece of flat Pyrex glass, which required a flat nose and a drag-reducing windshield on the missile. The penalty in drag for a blunt nose shape is more than offset, at least at the higher altitudes, by the increased range over which the guided rocket, as compared with the unguided rocket, may be successfully used due to its homing capabilities.

It was recognized from the beginning that one of the primary problems would be that of resonance encountered when the roll frequency corresponds to the pitch frequency. Because in the present case the dynamics are further complicated by the fact that the model is composed of two sections rolling at different rates, it was arbitrarily decided to restrict the missile to operation with the roll frequency less than the pitch frequency for the first test flights. This necessitated a pitch frequency as large as possible, which resulted in the canard configuration with the wings as far to the rear of the rocket as possible.

The wings have a 60° triangular plan form with the tips of two wings cut off to provide mountings for tracking flares. The cruciform wing arrangement was required, because the roll angle of the rear end is not controlled and thus essentially equal lift must be developed at all roll attitudes. To avoid nonlinear aerodynamics and induced rolling moments (dihedral effects) on the forward surfaces it was decided to limit the operating region for the model to an angle-of-attack range no greater than 5°. The wing size was chosen to produce a useable normal acceleration (about 2.5g) at 40,000 feet altitude at this angle of attack.

The first models flown utilized 60° triangular canard surfaces, as mentioned previously, primarily because the aerodynamic characteristics of such surfaces at low supersonic speeds were fairly well known. Although a single set of surfaces would have been sufficient to perform both the pitch and roll control functions, the cruciform arrangement was adopted to provide sufficient aerodynamic roll damping, while keeping the span and area and thus the pitch destabilizing effect of the canards to a minimum. Several difficulties were encountered with these surfaces, however. For the low rates of roll desired, only about $\pm\frac{1}{2}^{\circ}$ deflection

of each all-movable aileron was required; and accidental play in the system due to construction tolerances and wear during instrumentation and preflight checkout resulted in large deviations from the desired deflections. During one flight test with the triangular canards, the rolling velocity was variable during each revolution of the head, leading to the suspicion that the induced rolling moments of the 60° swept surfaces were appreciable. The design of the canard surfaces was therefore changed to an unswept tapered plan form to reduce the induced roll effects, with trailing-edge ailerons to permit larger deflections (about 5°). Subsequent wind-tunnel tests showed that the variable roll velocity could also have been caused by bearing friction. The roll bearing was therefore redesigned to reduce friction.

A flight test of a model with the modifications described above was made and revealed another difficulty. At low speeds during the initial acceleration, the lift and pitching accelerations developed at such rates as to cause the model to turn before the roll velocity and acceleration had reached rates sufficient to orient the lift vector in the direction of the target. Therefore, a lift-cancellation flap was designed for the pitch canards (fig. 4(d)) which, when deflected at the correct angle in the opposite direction from the pitch canards, results in complete cancellation of the lift at subsonic speeds while permitting the desired amount at supersonic speeds. This device would also be advantageous for air launching of missiles from subsonic airplanes since it would assure that the missile would remain at zero lift until well clear of the airplane. This device, of course, imposes the restriction that only the supersonic portion of the flight is available for maneuvering, but for ground-launching of the present test it permits a greater assurance of target acquisition.

Aerodynamic Characteristics

No complete series of tests has been made to define the aerodynamics of the configuration. Only those tests have been made which were felt to be necessary to insure satisfactory operation of the system. The aerodynamic data to be presented were obtained, partly from a limited number of wind-tunnel tests of the forward rolling section only (no rocket or wings) in the Langley 7- by 10-foot high-speed tunnel and the Langley 4- by 4-foot supersonic pressure tunnel, partly from flight tests of complete models, and partly from estimations based on other data.

Drag.- The drag coefficients for the model as obtained from Doppler radar data are shown as a solid line in figure 6. The curve shown has been corrected to zero lift by subtracting an increment $\Delta C_D = \frac{C_N^2}{C_{N_\alpha}}$, but this correction was very small. Also shown by the dashed line in

figure 6 is the drag of the canard missile configuration of reference 3. The drag of the present model is considerably higher than that of the missile and this is believed to be due primarily to the nose shape. It is probable that some developmental testing of other nose or windshield arrangements would result in drag reductions.

Lift.- Lift-curve slopes of the complete model and various model components are shown in figure 7. The solid curve, for the complete model, was obtained from the trim lift and angle of attack of a model having the triangular canard surfaces. When the triangular surfaces were replaced by unswept surfaces the aspect ratio and area of the unswept canards were chosen to give approximately the same lift-curve slope and damping in roll as the triangular surfaces. To apply to the complete configuration the solid curve in figure 7 also involves the assumption that the total lift produced by canard deflection $\left(C_{L_{\delta_c}}\right)$ is zero. Data for a similar configuration in reference 4 and calculations for this model indicate that this is a good assumption, because the lift on the canard surface due to deflection is opposite in sign and very nearly equal to the increment in lift on the wing caused by downwash from the deflected canard.

The other curves in figure 7 show the lift on the canard surfaces and the forward section of the model (no wing present) caused by angle of attack $\left(C_{L_\alpha}'\right)$, pitch canard deflection $\left(C_{L_{\delta_c}}'\right)$ and flap deflection $\left(C_{L_{\delta_f}}'\right)$. The long-dash curves are faired values used to estimate static stability and control effectiveness. The greater proportionate loss in lift effectiveness of the flap compared to the canard as the speed increases (fig. 8) is the factor utilized in the subsonic lift-cancellation scheme.

Static stability.- The static stability margin is about 30 inches. Variations from this amount, caused by Mach number effects and rocket burning, are a maximum of about 4 inches.

Pitch control effectiveness.- The pitching-moment effectiveness of the canard surface is given in figure 9. The curves represent estimated values based on the wind-tunnel lift data of figure 7 and estimated downwash. The higher curve is for the condition where no flap deflection is used. The lower curve has a ratio of flap deflection to canard deflection of -1.90, which is the value that will produce essentially zero canard lift and thus zero model lift at Mach numbers below about 0.6. With the use of this ratio only about a 25-percent increase in canard deflection is required to produce the same supersonic lift as produced with no flap deflection.

Aileron effectiveness.- The aileron effectiveness is shown in figure 10, the upper curve being for the aileron extending to the trailing

edge of the canard surface. The long-dash curve is again a fairing used for estimation purposes. In addition to the rolling effectiveness measurements, free-rolling tests were also made with this aileron in the 4-foot tunnel. These tests showed rolling velocities greater than anticipated or desired. Since the control system mechanism on the model had already been assembled and adjusted for flight it was judged more expedient to reduce the aileron chord to obtain the desired rolling velocity rather than to disassemble the model to change the control deflection. The aileron chord was therefore shortened for the flight model as shown in figures 3(b) and 4(c) and an estimate of the reduced effectiveness is shown by the short-dash line in figure 10. Reference 4 was used to estimate the reduction in effectiveness.

During the aileron effectiveness tests in the 4-foot tunnel a rolling-moment variation with angle of attack at 0° aileron deflection was observed, as shown by the curve with diamond symbols in figure 11. No reason for this was apparent until it was noticed that the nose had been installed such that the legs of the tripod supporting the windshield (fig. 5) had been placed so that they were unsymmetrical with respect to the angle-of-attack plane, as shown by the small sketch. When the nose was rotated 180° the rolling-moment asymmetry was also altered as shown in figure 11. It is probable that the effect shown is not a rolling moment on the tripod itself but is caused by an unsymmetrical airflow over the canard surfaces. For subsequent flight models the tripod was replaced by an octapod (fig. 4(b)).

TEST CONDITIONS

Model Instrumentation

Two systems of instruments were incorporated in the missile. The seeker and control system was used to guide the missile toward the target. The telemeter system functioned to measure and monitor the performance of the missile under the action of the control system.

Seeker and control system.- The guidance principle requires that the bearing-mounted section of the missile reverse its roll direction each time that the resultant lift vector, produced by the fixed lift surfaces, crosses the missile-target line of sight. In this manner the flight path is corrected to reduce the angle between the missile-target line of sight and the missile's flight path whenever the target appears in the field of view and outside the small central dead cone as discussed previously and shown in figure 2.

In order to accomplish this, a simple infrared detection system was used with the appropriate controls to position the ailerons for either

clockwise or counterclockwise rolling. A block diagram of this system is shown in figure 12.

The optical system which was used consisted of a flat glass window with suitable infrared transmission properties and a spherical mirror to reflect to a lead sulfide infrared detector. Since pursuit navigation was used, as stated previously, it was not necessary to use gimbals and all parts of the optical system were mounted directly to the forward section of the missile. The glass window was protected by an octapod mounted windshield as shown in figure 4(b).

The amplifier and control circuits used to operate the actuator for positioning the ailerons are shown in figure 13. Tests were made with radiation sources of the same type as the target in order to determine the proper operating gain for the system and to determine that the dynamic range of the amplifier was adequate.

The system was set up to reverse the deflection of the ailerons each time the target left the instantaneous field of view. This was done to preclude the possibility of the missile's reversing roll direction before the target was outside the field of view. This results in less efficiency since the resultant lift vector must rotate through a larger angle than would be required if the aileron deflections were reversed each time the target entered the field of view. Under steady-state hunting conditions, this additional angle corresponds to twice the duration of the signal voltage produced by the target.

Measurements made with the same type of radiation source that was used as a target indicated that the quality of the optics and other factors were such that the signal voltage produced by the target had a duration equivalent to 0.07 to 0.15 of a revolution of the rolling section of the missile. At a range of 500 feet this duration was found to correspond to 40° of rotation of the bearing-mounted section throughout practically the entire field of view. Thus, under steady-state hunting conditions at a range of 500 feet, the lift vector must rotate through an angle 80° greater than would be required if the aileron deflections were reversed each time the target entered the field of view.

Other important system parameters which were measured are:

The instantaneous field of view, deg	$1^{\circ} \times 5^{\circ}$
Response time for full reversal of aileron deflections, sec . .	0.01

It should be noted that this equipment was designed solely for the purpose of testing the homing system principles. Background discrimination, against sharp-edged clouds or other extraneous signal sources, such as would be required for tactical use was not obtainable with this test equipment. To reduce interference from the background and to provide maximum target contrast the system tests were conducted at night.

Telemeter.- Standard NACA radio telemetry was used. The following quantities were recorded: roll angle of control end with respect to aft end; aileron position; and missile acceleration components, measured by accelerometers in the plane of the roll reference and the plane perpendicular to the roll reference.

Ground Instrumentation

The object of the ground instrumentation was to provide information from which relative distance between missile and target could be determined. In addition to the standard radars used to measure missile velocity and position, photographic and radar coverages were provided so that target position could be determined.

Target Characteristics

Because of the seeker acquisition difficulties encountered when ground-launched models are used for test purposes, an essentially stationary target was chosen. A parachute flare was ground tested to determine if proper illumination levels were obtained at the slant range to be encountered throughout the flight test. These tests showed that this flare appeared to offer suitable characteristics for our purposes.

As mentioned previously, the flight test was conducted at night so that a minimum of background interference would be encountered. The airplane used to drop the flare was vectored into position by ground control radar. The flare location was specified as, slant range from the launcher of about 5,700 feet, elevation angle 60°. This target location allowed the use of the missile throughout the supersonic flight range.

Launcher

Since the exact position of the target at the moment of launching could not be predicted, it was necessary to use a trainable launcher aimed so that the seeker would acquire the target when the missile reached operating speed. A rail-type launcher 4-feet long was mounted on a modified servo-controlled searchlight base as shown in figure 14. The servos were controlled by an optical sight. Thus the rail and missile on the rail could be aimed properly.

Trajectory calculations and experimental tests of previous models showed that if the target was at an elevation angle of 60° to 75° an intentional misalinement of 6° between optical tracker and rail launcher should be used. This correction in aim point was necessary to allow for the gravity drop and tip off of the missile as it came off of the rail launcher.

RESULTS AND DISCUSSION

An unguided model was launched to verify the 6° launcher correction angle. Radar plots of the flight path confirmed the value chosen. This model missed the target flare by approximately 600 feet. A photograph of the trajectory, shown in figure 15(a), was made by opening the shutter of a still camera and allowing the paths of missile flare and target flare to be recorded as lines during the flight.

Homing System Performance

On the basis of the unguided model test the same correction angle was used during the launching of the system missile. The wind at ground level was less than one mile per hour for both launchings. The telemeter record showed that target acquisition occurred shortly after take-off and the seeker hunted for one and one-half cycles. Operating velocity had not been attained however, so that negligible trajectory curvature occurred, since the lift-cancelling flap was effective. The lift increased to about one-half "g" toward the end of this initial hunting sequence. Evidently due to pitching moment, the missile heading error was reduced and the missile was pointed in a direction to reduce the launching error and cause the target image to enter the seeker dead spot. The seeker then rolled continuously until the missile-target range was about 1,250 feet. At this point the seeker again hunted on the target.

The flight-path curvature which occurred during the second hunting interval is noticeable on the trajectory photograph of figure 15(b). Comparison of the unguided model trajectory and the guided trajectory allows the amount of correction due to the homing system operation to be determined. The ground instrumentation showed that all the correction took place in the plane of the photograph of figure 15(b). Direct comparison of figure 15(a) and (b) will then show the amount of correction. To facilitate this comparison a composite photograph of the unguided model and system test-missile trajectories is presented in figure 16. The launching angle for the two trajectories differed by about 8°. The path of the system test missile, figure 15(b), was rotated by this amount to allow comparison of the two trajectories in figure 16.

The distance between the two trajectories at the intersection of the target flare path and system test-missile trajectory represents the amount of correction. Since the target slant range is known, this distance may be determined by proportion and is found to be 130 feet. The closest relative distance between missile and target is determined in the same manner and is 90 feet. This figure is confirmed by measurements made using the other ground instrumentation.

For the missile-to-target velocity ratio used during this flight test (approximately ∞ since the target was almost stationary), it would be expected from theoretical studies (ref. 5) that the missile would miss the target. This is expected since an infinite missile rate of turn is required when the missile-to-target velocity ratio exceeds 2.0 for pure pursuit navigation. For a more favorable velocity ratio, such as would be encountered in the tactical application of a missile using this principle, more time to correct the trajectory would be available and a smaller miss would be produced. However, the fact that the seeker hunted on the target and that a 130-foot flight-path correction was produced leads to the conclusion that the fundamental operating principle is sound.

Although the model experienced accelerations of about 7 "g's" during the steady rolling period prior to the final hunting period, the helix produced by this motion had a diameter of less than one foot, which is too small to be apparent on the flight-path photographs of figures 15 and 16.

The components of missile acceleration which were telemetered were reduced to an acceleration vector. The locus of the tip of this vector is shown in the polar plots of figure 17(a) and figure 17(b). The scanning action which occurs during continuous rotation of the head produces the spiral enclosing trace. After acquisition occurs and hunting begins the acceleration trace takes on the shape of the bent figure eight in the center of the plot.

The switching points (where the seeker saw the target and reversed the aileron deflection) are marked on this curve. Since the acceleration reference is to the aft end of the body and the switching points are a space reference to the target, the angular separation of the switching points should be equal to approximately twice the signal width (about 80°) as explained in the description of the "seeker and control system" section of the report. The fact that this separation is of the right order of magnitude indicates that the rolling motion of the aft end was very slight or nonexistent. This switching-point separation also may be seen from a comparison of the relative roll-angle plot and the aileron-deflection plot presented in figure 18.

From the acceleration plot and the roll-angle plot, the roll hunting amplitude can be seen to be varying from $\pm 100^{\circ}$ to $\pm 115^{\circ}$. If the switching-point separation were minimized by using the leading edge of the signal, it appears that satisfactory roll hunting of a much smaller amplitude would be obtained.

Aerodynamic Performance

Figure 19 shows a curve (solid line) of Mach number against time for the ground-launched model as measured by radar. The maximum Mach number attained was 1.36 and the model remained at supersonic speeds for only 3.7 seconds. As noted previously, this is the time which the model has available for maneuvering. Also shown on figure 19 are curves calculated, assuming the model to be air launched at sea level and at 40,000 feet altitude with an initial Mach number of 0.6. At sea level, duration of the supersonic portion of flight is increased to 6 seconds, but the greatest improvement is obtained by operating at higher altitudes where the high drag is of less importance. The curve for 40,000 feet may be considered as the maximum performance at this altitude and was calculated for the same angles of attack at sea level, which would represent little or no maneuvering.

Figure 20 shows curves of range against time derived from the Mach number curves of figure 19. For the ground-launched model the range for successful maneuvering is less than 6,000 feet. Launching at 0.6 Mach number at sea level would permit an operating range of about 9,500 feet, while launching at 40,000 feet would permit maneuvering flight to maximum ranges of the order of 35,000 feet.

It can be seen that the choice of ground launching for the model test severely limited the time and range over which the model could demonstrate successful operation. The ground launching was justified on the basis of the greater simplicity, reliability, and accuracy of the ground-based check-out, launching, and tracking procedures.

Figure 21 shows in time-history form the average normal accelerations experienced by the model during the flight test, and figure 22 shows the same data converted to normal-force coefficients and plotted against Mach number. The data shown are mean values through oscillations. In the hunting portion of the flight at supersonic speeds the values shown are the approximate average accelerations in the direction of the average roll angle. During this period the model experienced rather large accelerations normal to this direction caused by the hunting action, as was shown in the polar plot discussed previously, but these accelerations had an average value near zero. In both figures 21 and 22 the short-dash lines indicate values estimated from previously discussed stability and control effectiveness data for the condition of zero rolling velocity.

Large amplifications of acceleration as caused by the steady rolling velocity are apparent. During the hunting period the acceleration agrees fairly well with the estimated values. The action of the lift-cancellation flap at subsonic speeds is apparent in figure 22 also. The differences exhibited by the normal-force values during accelerating and decelerating flight (indicated by the arrows in figure 22) represent the dynamic response in pitch of the model to the disturbing aerodynamic and inertia

moments. The flight time illustrated by the solid curves is about 1 second for the accelerating part and 5 seconds for the decelerating part.

Roll-pitch dynamics.- The rolling velocity of the nose section of the model with respect to the rear section is shown by the solid lines in figure 23 for the steady rolling portions of the flight. Since the rear end of the model apparently had little or no rolling velocity (see section on "Homing System Performance") this curve represents the absolute rolling velocity of the nose section. The long-dash line shows the value, estimated by use of reference 4, for the ailerons alone. The flight values are somewhat higher at supersonic speeds than those estimated, and this can be explained by considering the alinement of the other canard surfaces. Both periods of steady rolling illustrated in figure 23 occurred with the nose section rolling to the right (clockwise when viewed from the rear). Measurements of the alinement of all surfaces immediately before flight showed that the 4 canard surfaces had an average misalinement of 4 minutes in a direction to produce right roll, and the 2 lift-cancellation flaps had an average misalinement of 30 minutes also in a direction to produce roll to the right. Estimations based on references 4 and 6 showed that the fin and flap misalinements would add about 5 and 4 radians per second respectively to the right rolling velocity at supersonic speeds.

The rolling velocity shows abrupt decreases at two points during the decelerating part of the flight. The reasons for this are unknown but it may be due to bearing friction or binding. The rolling velocities and rolling moments used are actually very small ($pb/2V = 0.01$, $l \approx 1.3$ ft lb) and small amounts of friction would have large effects. This kind of trouble was encountered during one of the series of wind-tunnel tests, leading to the redesign of the bearing section mentioned previously.

As noted earlier, the decision was made to operate the system with the steady roll frequency less than the pitch frequency. The curve of estimated pitch frequency in figure 23 shows that this objective was accomplished, but the difference between the two frequencies was not large, leading to the large amplification of normal accelerations discussed previously. Since the roll frequency varies very little with altitude, whereas the pitch frequency varies considerably with altitude (fig. 23), operation of the system in the present manner would result in the condition of roll-pitch resonance at some altitude higher than for the present flight test, unless the present small rolling velocity was further reduced. Also, since higher angles of attack than used in the present test would be required to produce sufficient acceleration at higher altitude (see fig. 24), the further amplification of these angles due to rolling at less than the pitch frequency would result in excessive attitudes. For these reasons it appears that for satisfactory operation at all altitudes it would be necessary to set the roll frequency higher

than the pitch frequency. This could be easily done with the present configuration by increasing the aileron chord and deflection and by moving the wings forward on the rocket. Further discussion and illustration of these roll-pitch dynamic effects is contained in the next section of this report.

Analog Studies

An important parameter which governs operation in this system is the ratio of rolling frequency to airframe natural frequency. The system was designed and the simulator studies of reference 2 performed with a rolling frequency equal to one-half the airframe frequency. To study further the frequency ratio obtained during the flight test, an analog simulation of the rolling lift vector and the airframe short period mode in the pitch and yaw plane was set up. From this setup, diagrammed in figure 25, records were obtained for a range of ratios and for a range of roll hunting amplitudes.

An illustrative sketch showing the manner in which the analog results were recorded is presented in figure 26. Polar plots of the vector angle of attack $\left(\sqrt{\alpha^2 + \beta^2} \angle \tan^{-1} \frac{\alpha}{\beta}\right)$ are plotted as a time locus during the steady rolling and hunting phases of operation. Representative results for rates of roll equal to 0.1 and 0.64 of the airframe frequency are presented in figures 27, 28, 29, and 30 for two hunting amplitudes, $\pm 60^{\circ}$ and $\pm 120^{\circ}$. All of the analog results are plotted to the same scale to facilitate comparison of the various conditions.

The magnification of angle of attack as resonance is approached is readily apparent. When ratios of roll to pitch less than one are used a considerable amount of wobbling of the airframe is incurred. This is undesirable since the drag will be considerably increased by such a useless gyration. However, the helix generated by this mode of operation is very small and so does not hinder system operation.

Comparison of the analog results and the flight-test results shows that the ratio of roll to airframe frequency obtained during the flight test was about 0.6.

Generally, a completely detailed comparison of the analog results (figs. 27 through 30) and flight test results (fig. 17) is not felt to be warranted. During the flight test several parameters which govern the character of the hunting oscillations were changing. For instance, the missile-target range, which influences both signal width and flight-path geometry, was decreasing rapidly; the trim lift was changing with Mach number; the Mach number was in the vicinity of 1.0 where aerodynamic coefficients may change rapidly; and a constant rolling velocity was assumed which was not the case during flight.

Additional analog computer runs were made with a ratio of rolling frequency to airframe frequency greater than one. Representative results are shown in figures 31 to 36. Obviously, this high-roll-rate type of operation is more efficient than the low-rate type which was flight tested, since the lift during the scanning or noncorrecting type of flight is very small but the lift during hunting is equal to a large percentage of the trim value. This means that the lift is large when required but small when not needed. The effect of a large hunting angle is to reduce the efficiency as may be seen from a comparison of the $\pm 60^{\circ}$ and $\pm 120^{\circ}$ portions of the figure. The dynamic operation of the system with large amplitude hunting is irregular, but no difficulty is apparent since the disturbances are less than trim. As a point of interest, it might be noted that in going from rolling to hunting or vice versa the airframe goes through the resonant frequency with no apparent difficulty.

This kind of operation was considered during the design and simulation stage of the project but was not simulated at that time. It was felt that the flight test could be conducted more expeditiously using the simpler roll control required for the low-roll rate. In view of the much more efficient operation which might be obtained with the high roll-rate, considerable promise for successful system operation under these conditions is indicated.

Suggestions for Future Research

Although this flight test proved that the fundamental principle of operation of the system is sound, it is apparent that several of the operating parameters were adverse rather than favorable. This leads to the suggestion that future research might be directed towards improving system operation by using a rolling rate higher than the airframe natural frequency. There are several advantages which will be reflected in the airframe construction from this type of operation. These are: increase of tolerance on aileron deflection, decreased effect of aerodynamic misalinement, and alleviation of altitude effects from airframe frequency change. Acquisition time will be reduced since the detection cone will be scanned at a greater frequency.

In the event that it is desired to improve operation with the low-roll rate, a considerable decrease in roll hunting amplitude may be obtained by causing the ailerons to reverse from the leading edge of the signal pulse.

CONCLUSIONS

A flight investigation at supersonic speeds of a simple homing system gave the following conclusions:

1. The somewhat unique principle of guidance and control exemplified by the simple homing system is fundamentally sound.

2. Considerable promise for system improvement is shown by a more favorable choice of operating parameters.

Langley Aeronautical Laboratory,
National Advisory Committee for Aeronautics,
Langley Field, Va., October 13, 1955.

REFERENCES

1. Gardiner, Robert A.: A Combined Aerodynamic and Guidance Approach for a Simple Homing System. NACA RM L53I10a, 1953.

2. Passera, Anthony L., and Garner, H. Douglas: Simulator Studies of a Simple Homing System. NACA RM L55G06, 1955.

3. Niewald, Roy J., and Moul, Martin T.: The Longitudinal Stability, Control Effectiveness, and Control Hinge-Moment Characteristics Obtained From a Flight Investigation of a Canard Missile Configuration at Transonic and Supersonic Speeds. NACA RM L50I27, 1950.

4. Strass, H. Kurt, Stephens, Emily W., Fields, Edison M., and Schult, Eugene D.: Collection and Summary of Flap-Type-Aileron Rolling-Effectiveness Data at Zero Lift As Determined by Rocket-Powered Model Tests at Mach Numbers Between 0.6 and 1.6. NACA RM L55F14, 1955.

5. Newell, Homer E., Jr.: Guided Missile Kinematics. Rep. No. R-2538, Naval Res. Lab., Radio Div., May 22, 1945.

6. Strass, H. Kurt, and Marley, Edward T.: Rolling Effectiveness of All-Movable Wings at Small Angles of Incidence at Mach Numbers From 0.6 to 1.6. NACA RM L51H03, 1951.

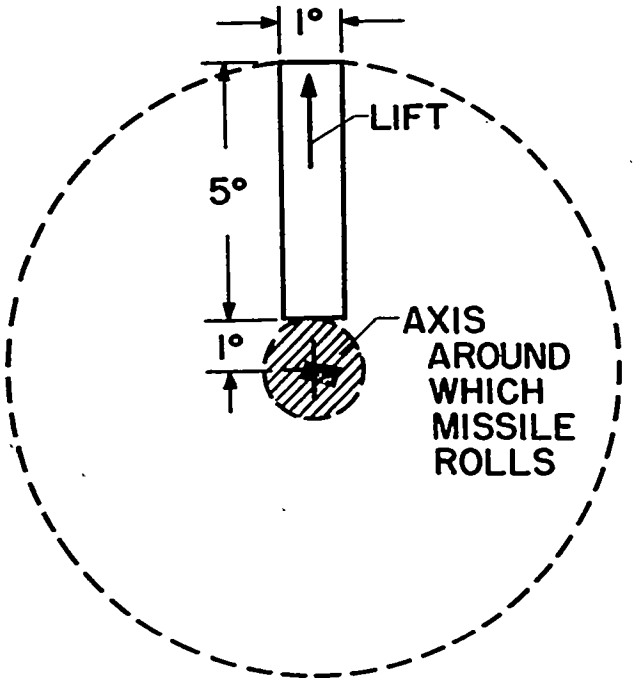

Figure 1.- Alinement of detection rectangle, lift, and axis around which missile rolls.

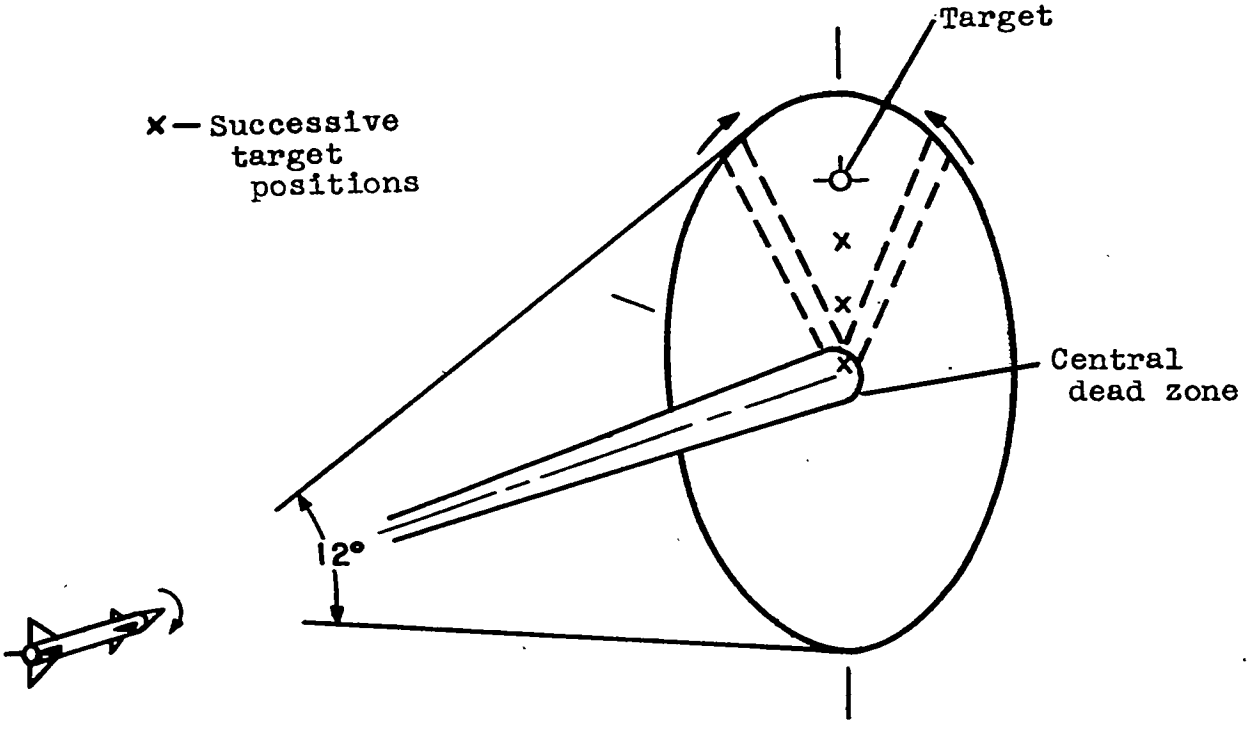

Figure 2.- Illustration of system operation.

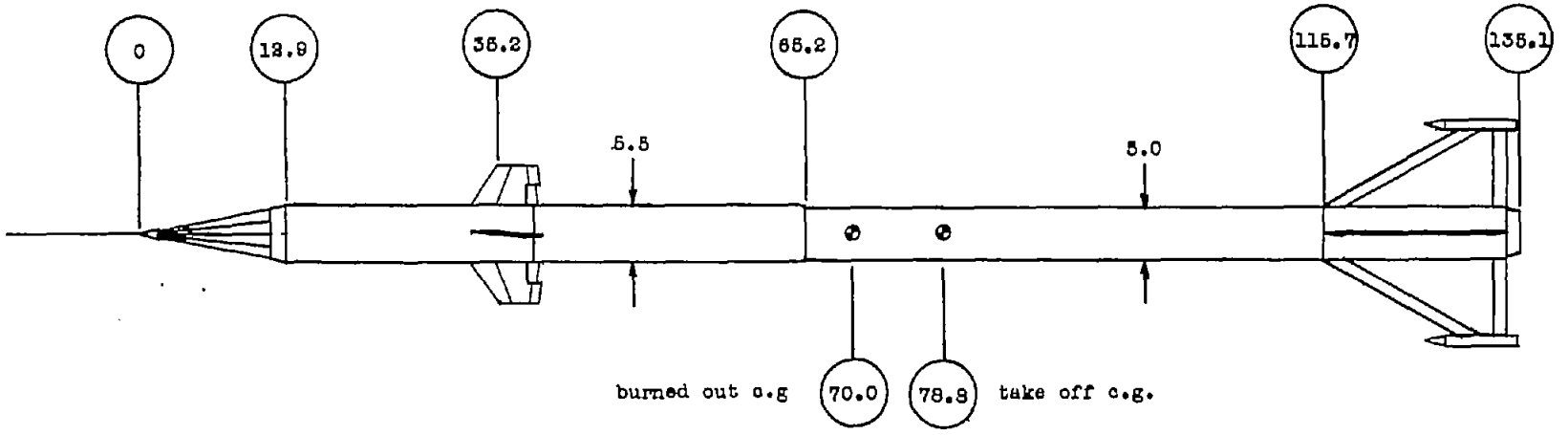

(a) Sketch of system test missile configuration. All dimensions are in inches.

Figure 3.- Sketch of model, wings, and control surfaces.

[redacted]

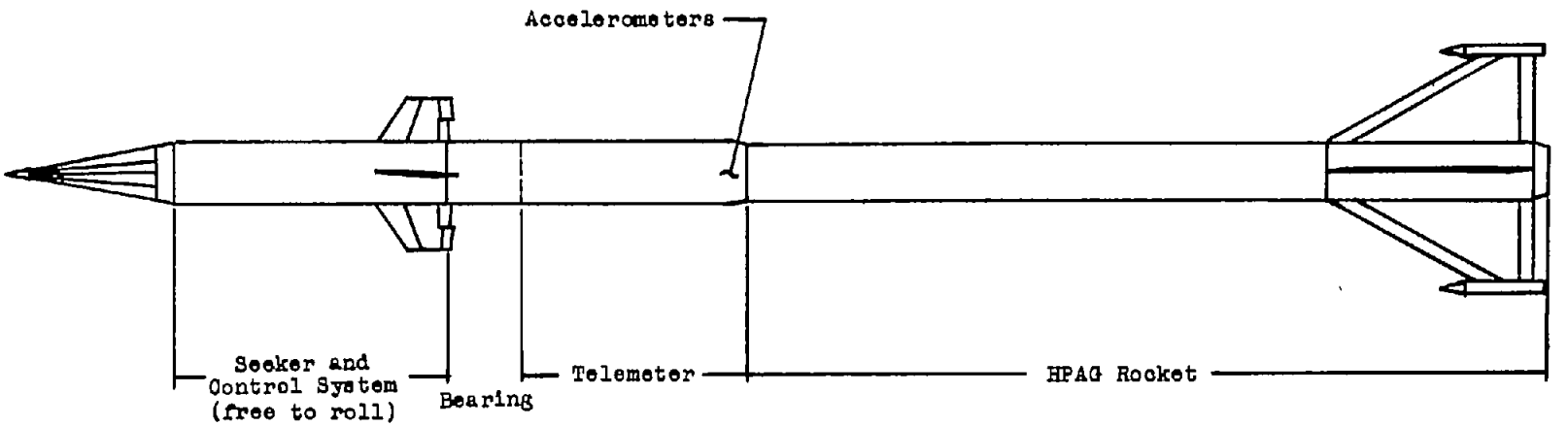

(b) Showing the location of the system test missile components.

Figure 3.- Continued.

[redacted]

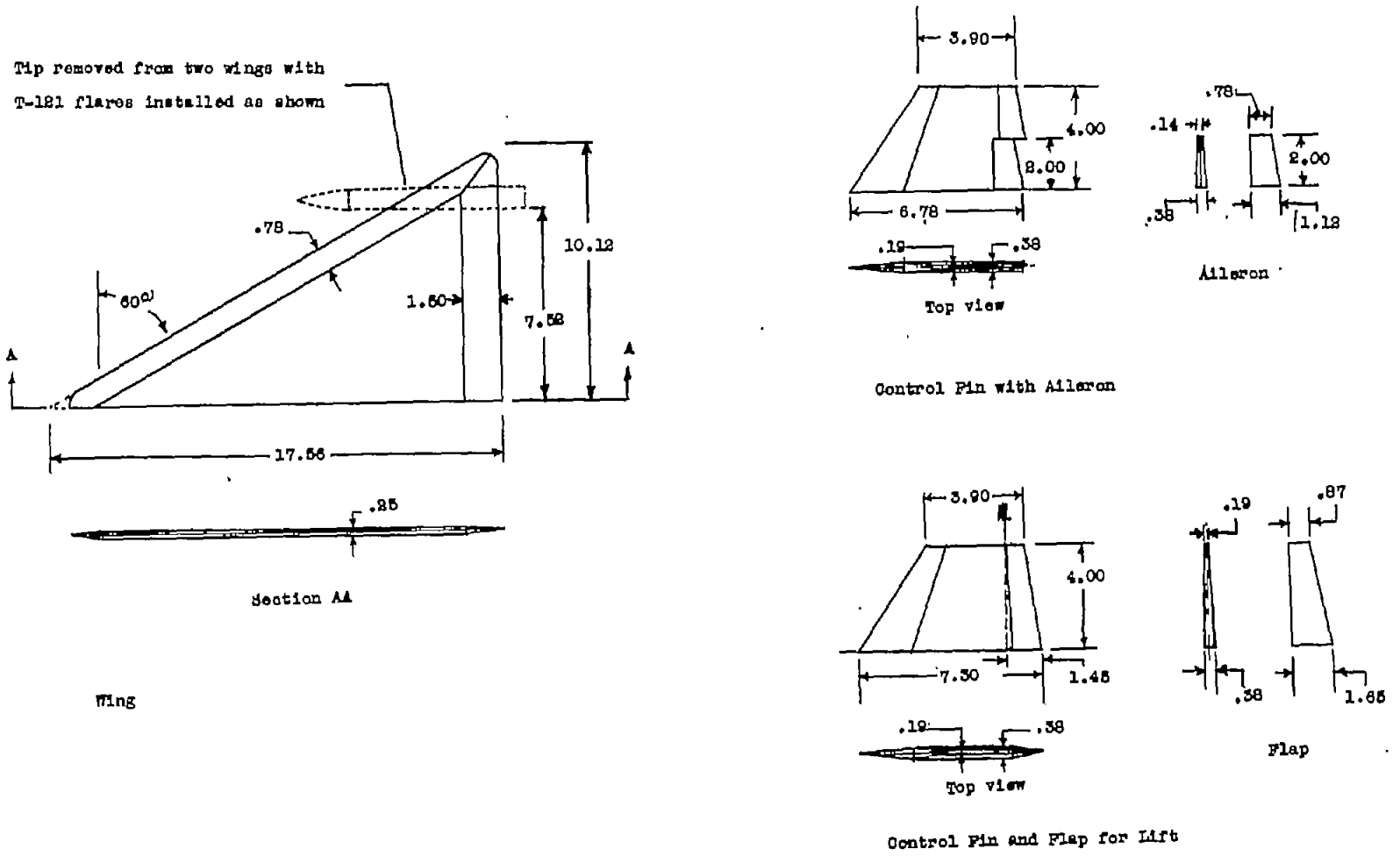

(c) Sketch of wing and control fins. All dimensions in inches.

Figure 3.- Concluded.

(a) Side view of model. L-87436.1

Figure 4.- Photographs of model.

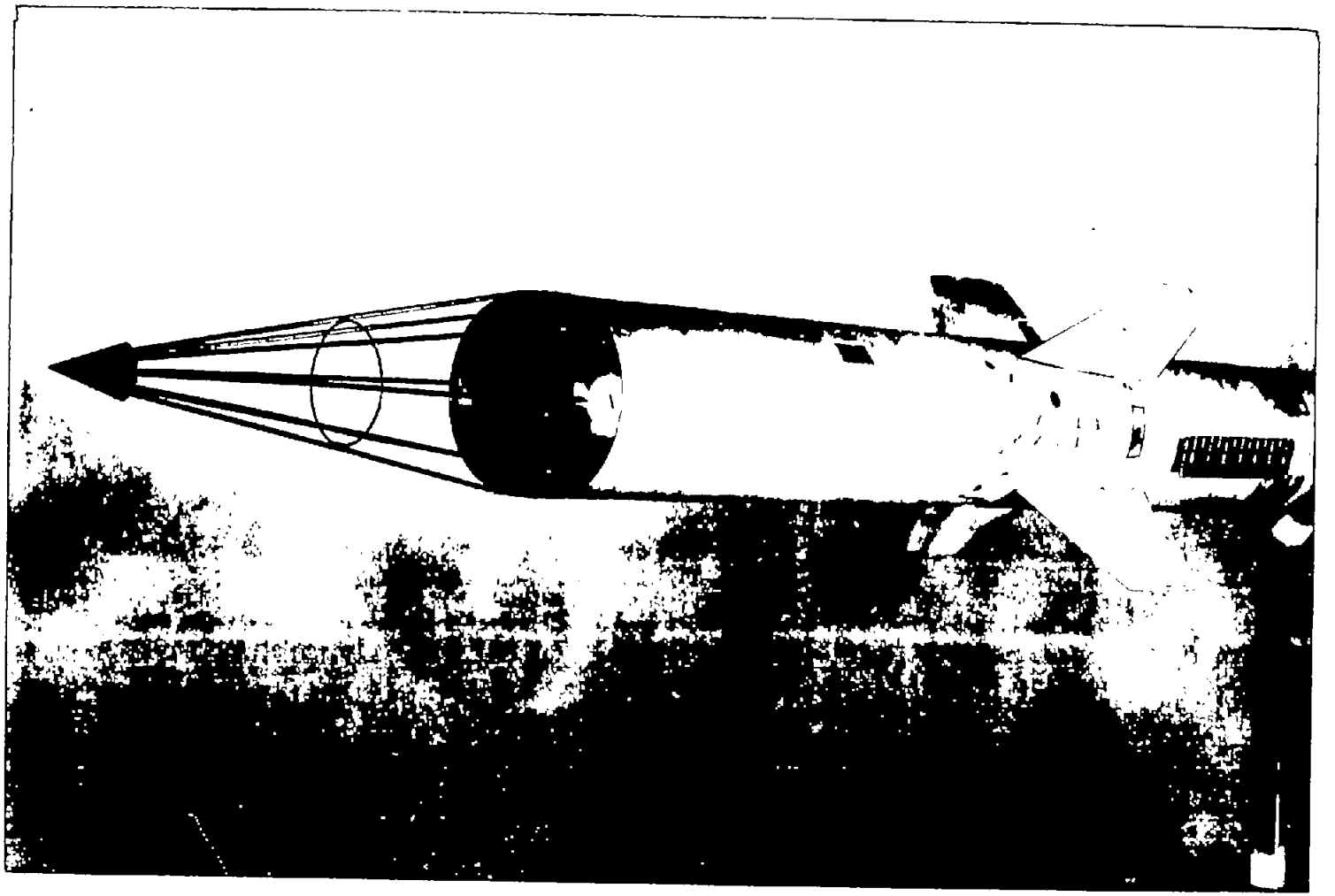

L-87439

(b) Model nose section.

Figure 4.- Continued.

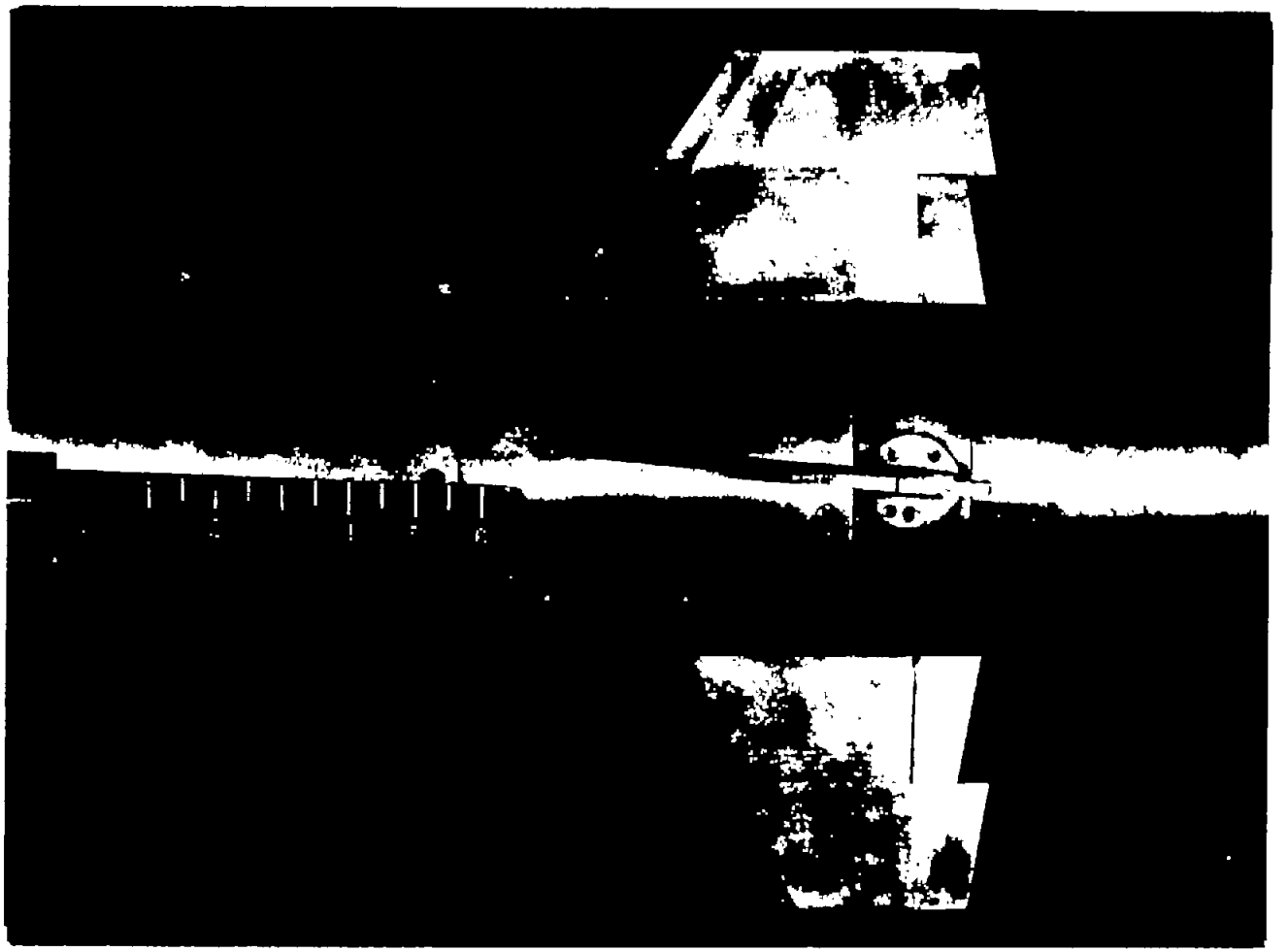

L-87440

(c) Plan view of canard surfaces with ailerons.

Figure 4.- Continued.

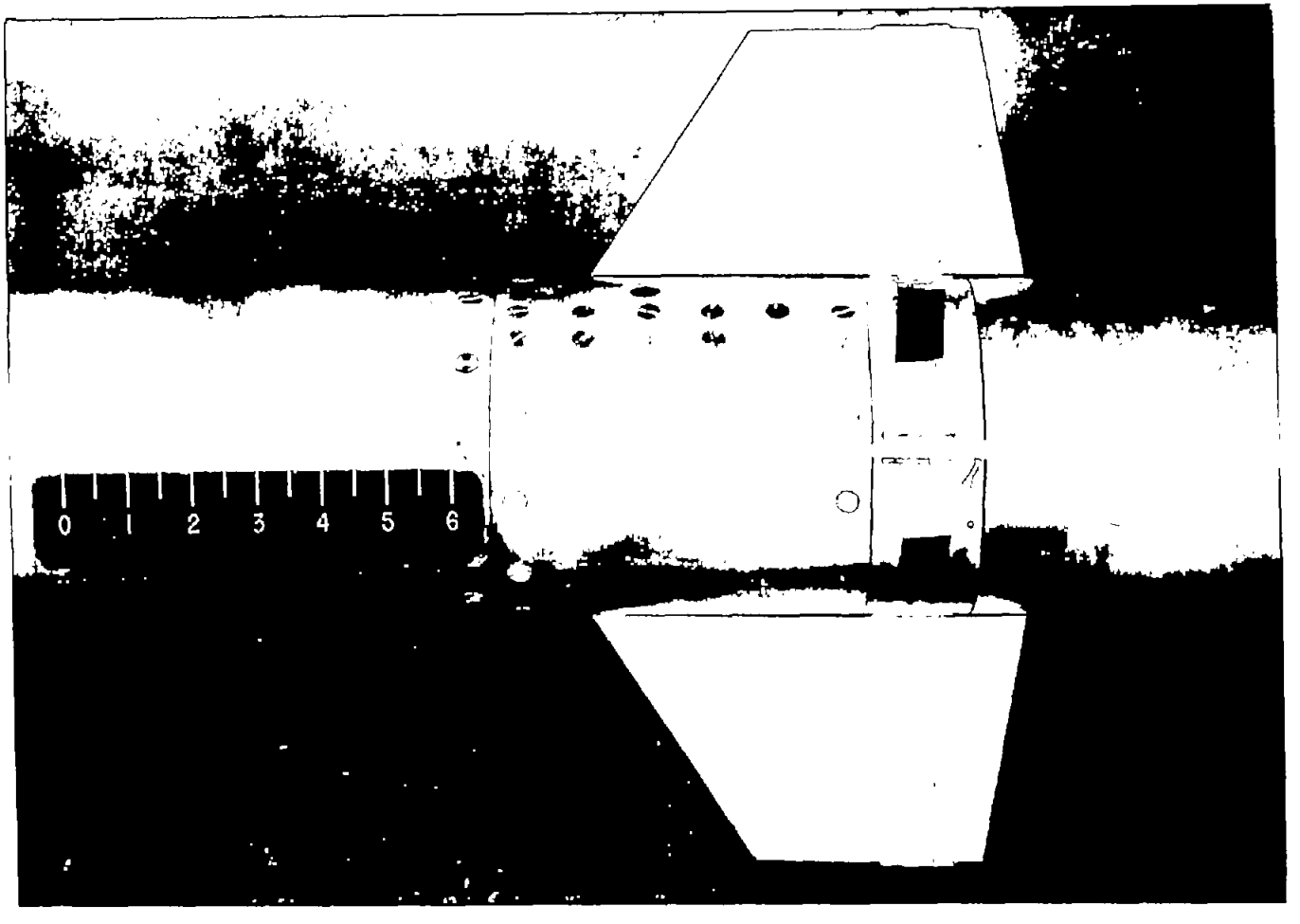

L-87437

(d) Plan view of pitch canard surfaces and flaps.

Figure 4.- Continued.

[redacted]

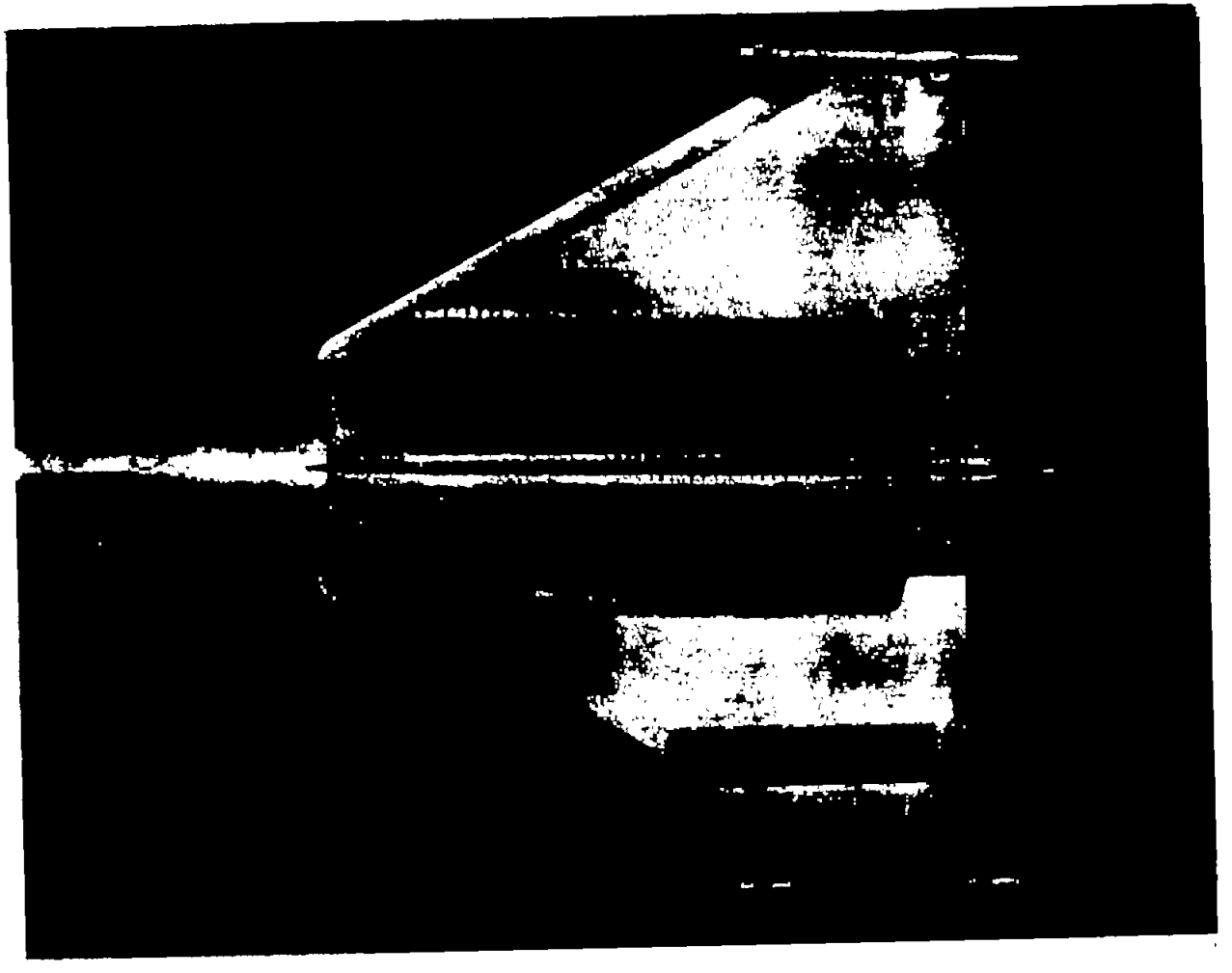

L-87438

(e) Model wings and flares.

Figure 4.- Concluded.

[redacted]

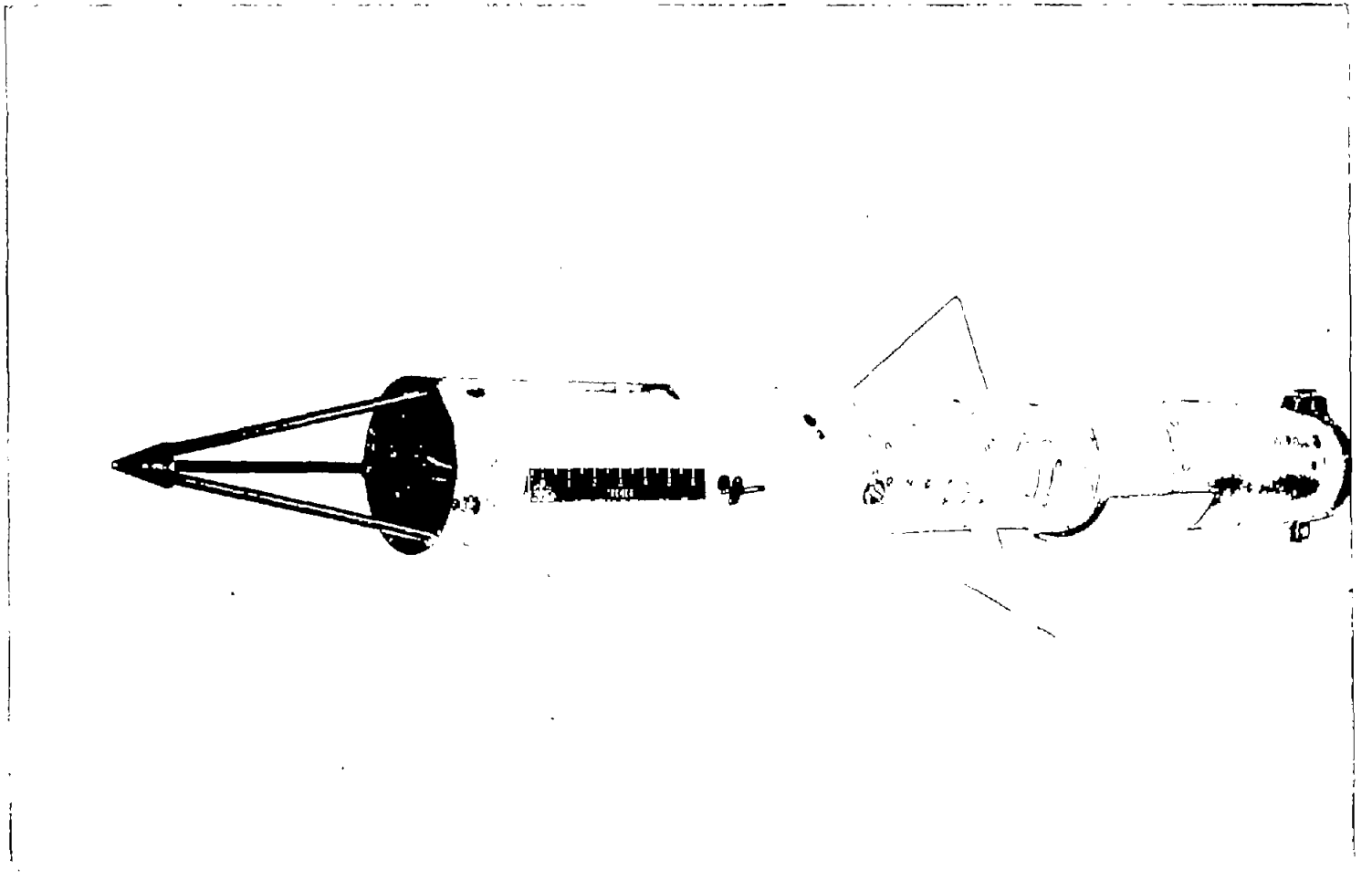

Figure 5.- Nose section before modifications.

L-81009

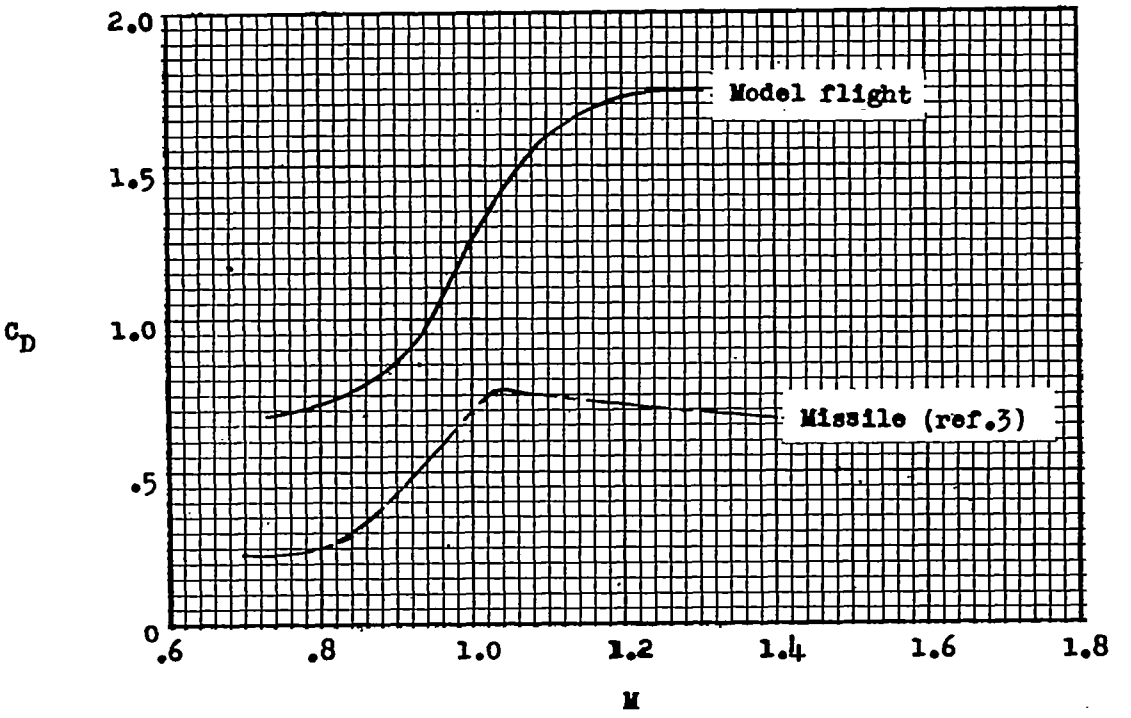

Figure 6.- Drag coefficients.

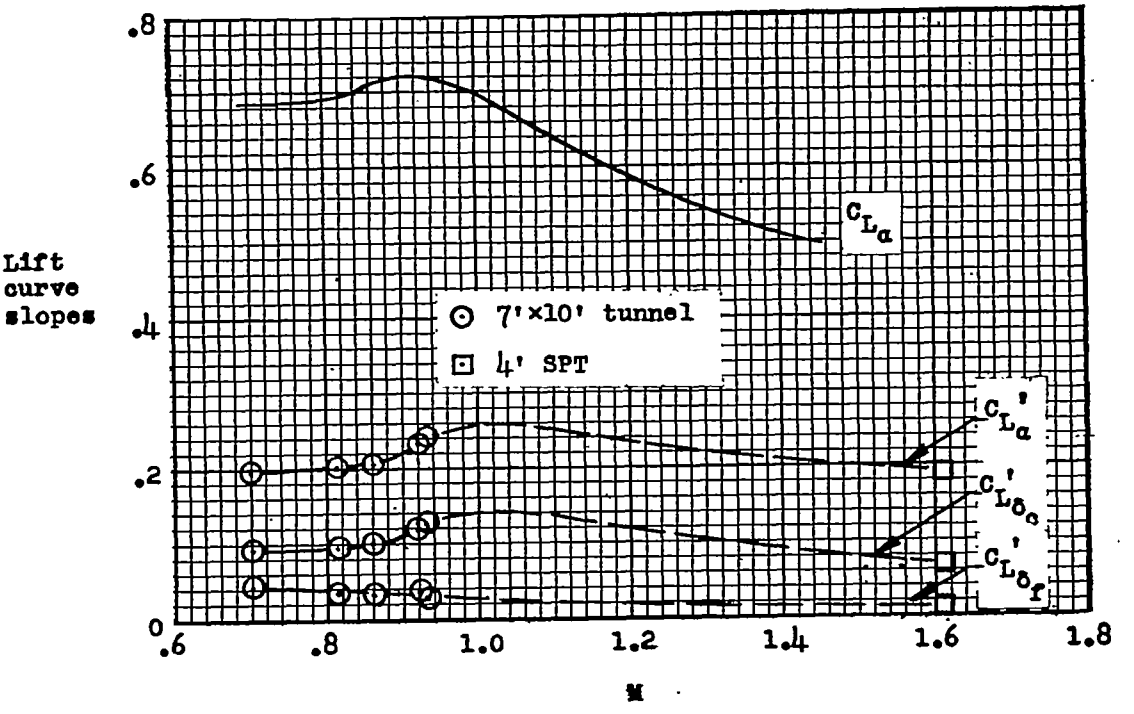

Figure 7.- Lift curve slopes.

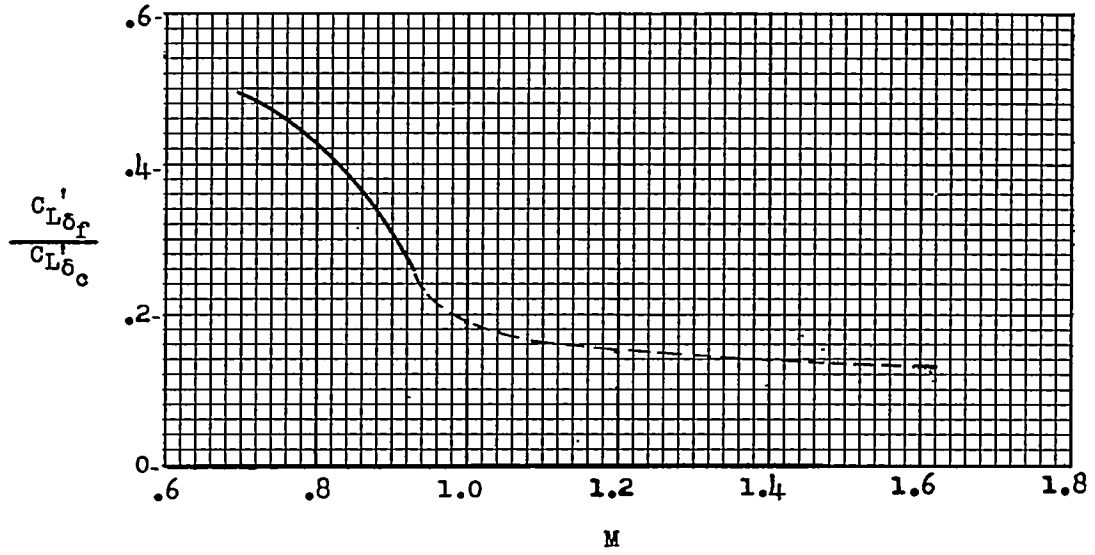

Figure 8.- Ratio of flap lift effectiveness to canard lift effectiveness.

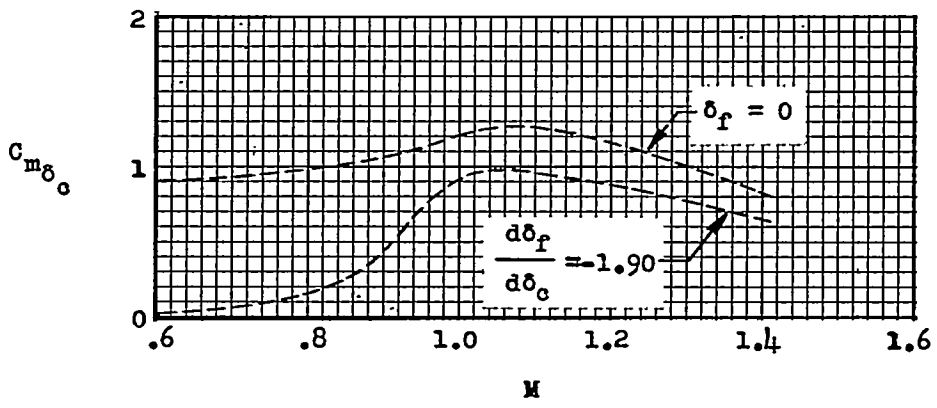

Figure 9.- Pitch control effectiveness.

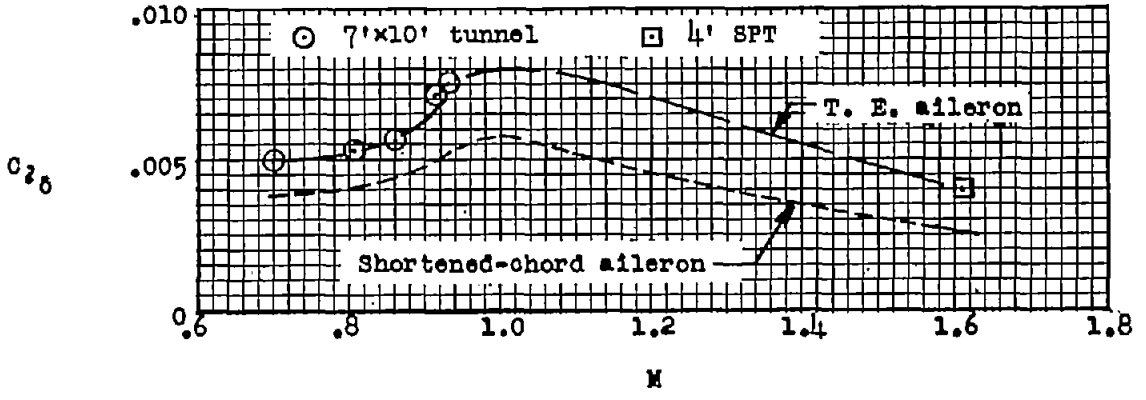

Figure 10.- Aileron effectiveness.

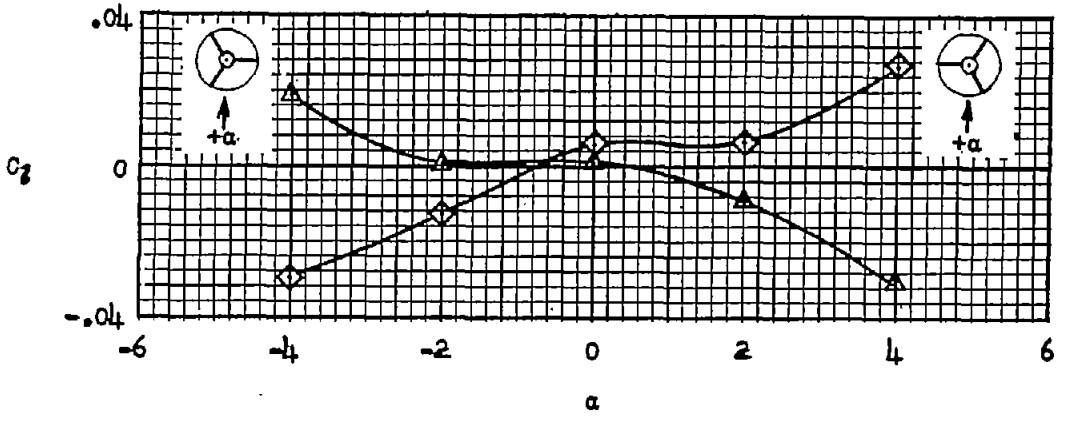

Figure 11.- Effect of nose tripod on rolling-moment coefficient at $M = 1.61$, $\delta_a = 0^\circ$. (Sketches show position of tripod legs.)

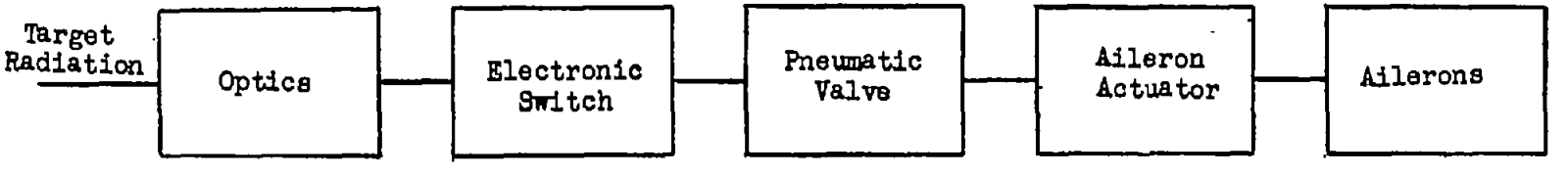

Figure 12.- Block diagram of seeker and control system used in flight test.

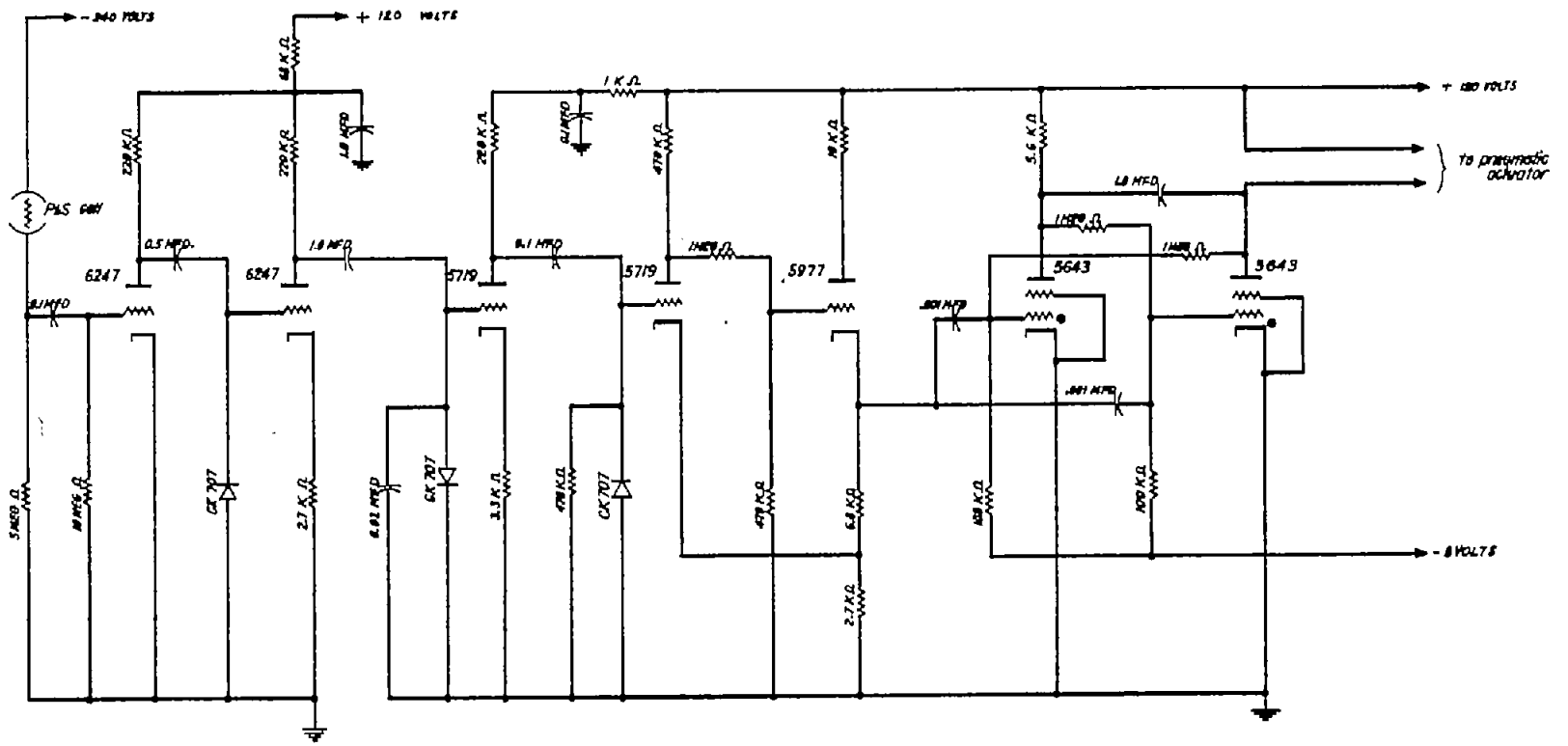

Figure 13.- Detector and amplifier circuit diagram.

L-83768

Figure 14.- Trainable launcher with model on rail.

[redacted]

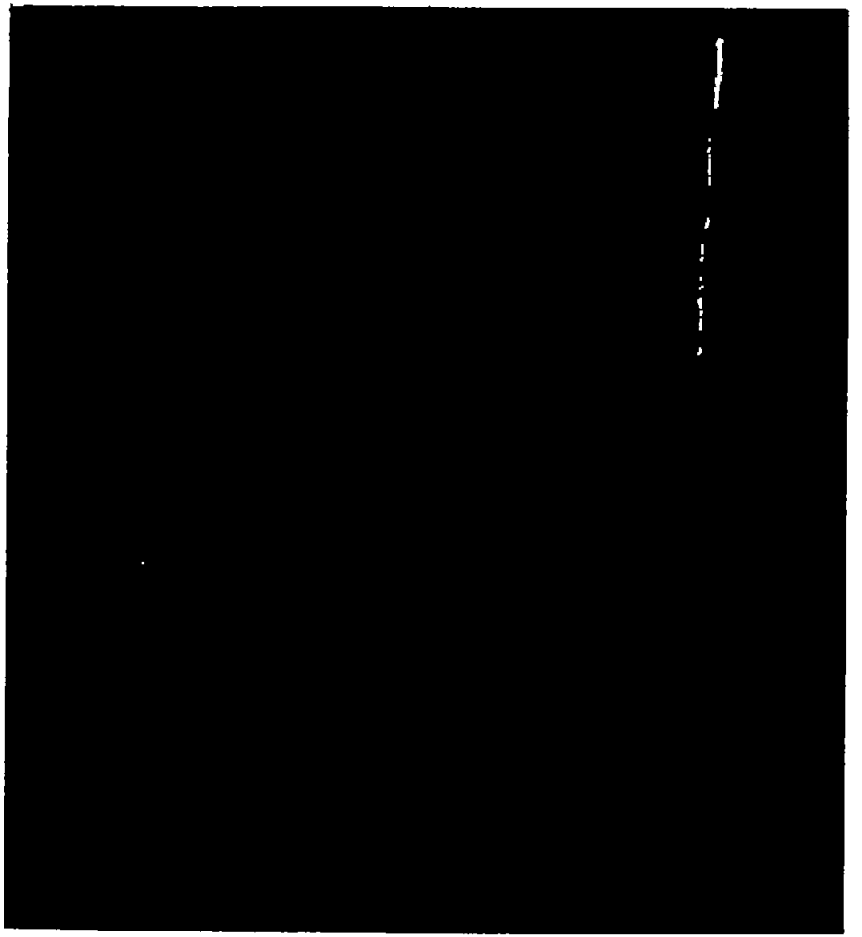

L-88940

(a) Unguided model. Slant range from launcher to target flare, 6,700 feet.

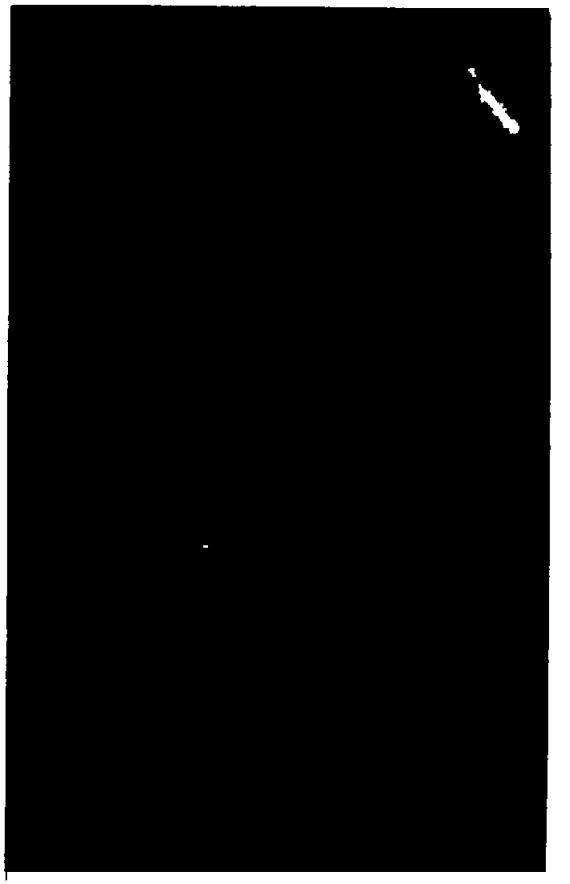

L-88941

(b) System test missile. Slant range from launcher to target flare, 5,925 feet.

Figure 15.- Photograph of path of missile flare and target flare.

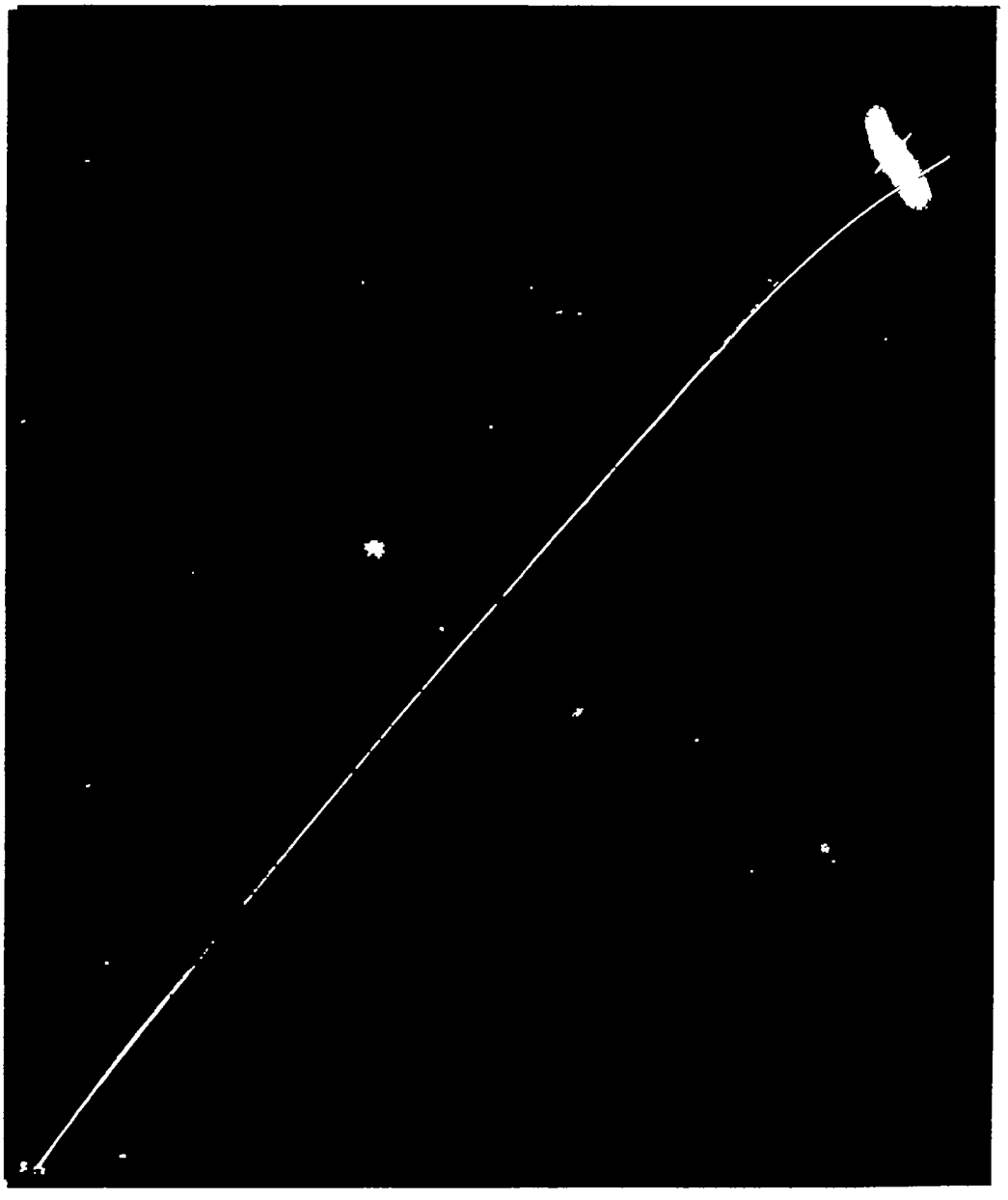

L-90557

Figure 16.- Composite photograph of unguided model and system test missile trajectories. Slant range from launcher to target flare, 5,925 feet.

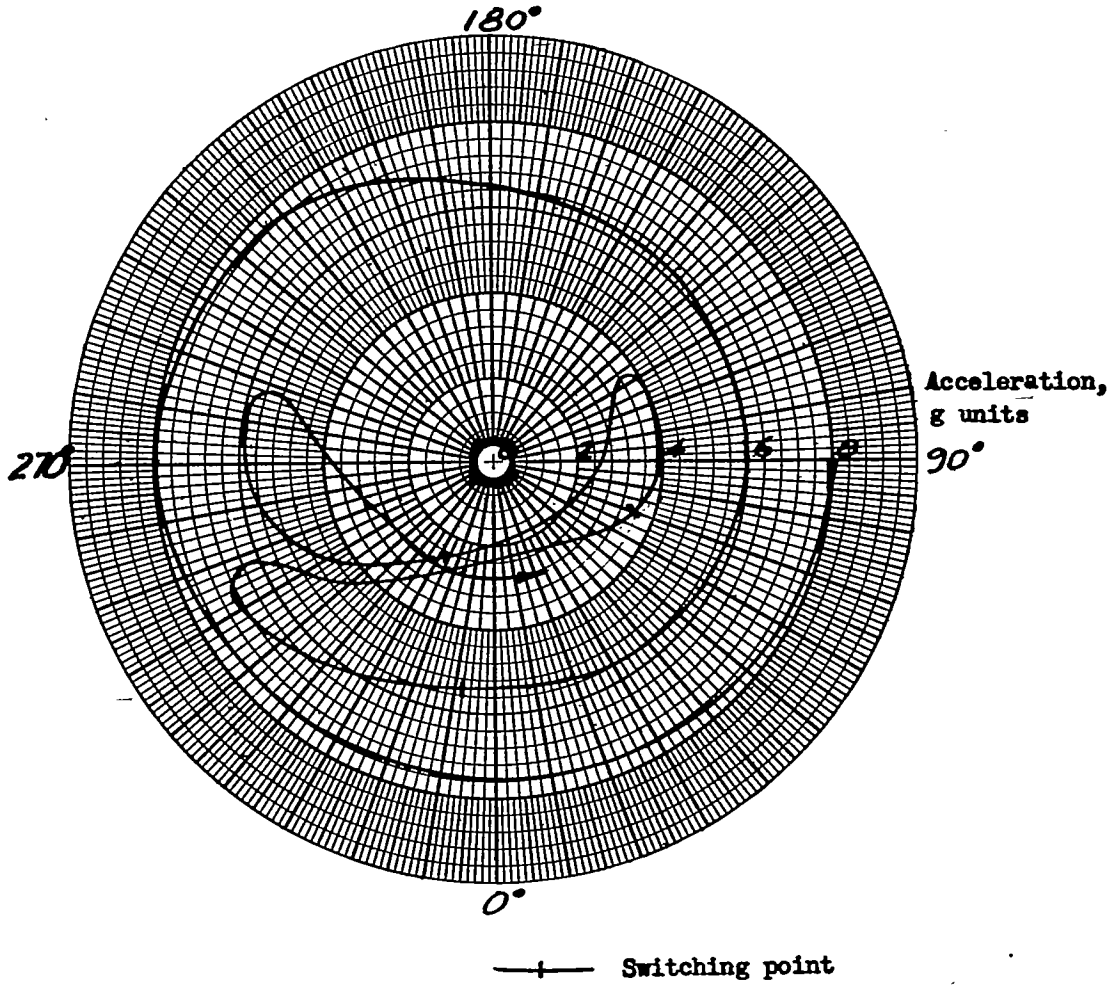

(a) Transition from rolling to hunting.

Figure 7.- Polar plot of locus of tip of resultant acceleration vector showing hunting during system flight test. Referenced to body axes of the rear end of the missile.

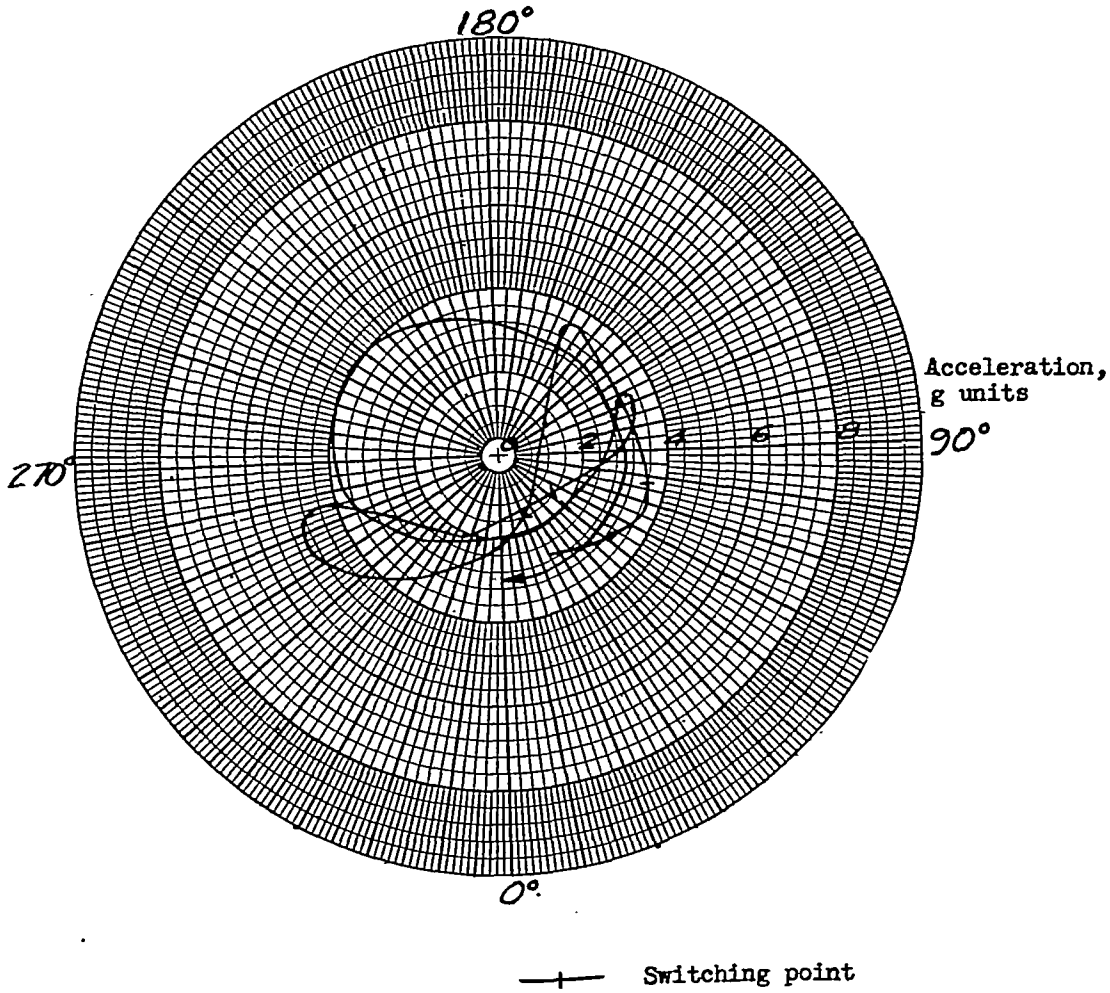

(b) Transition from hunting to rolling. Continuation of figure 17(a).

Figure 17.- Concluded.

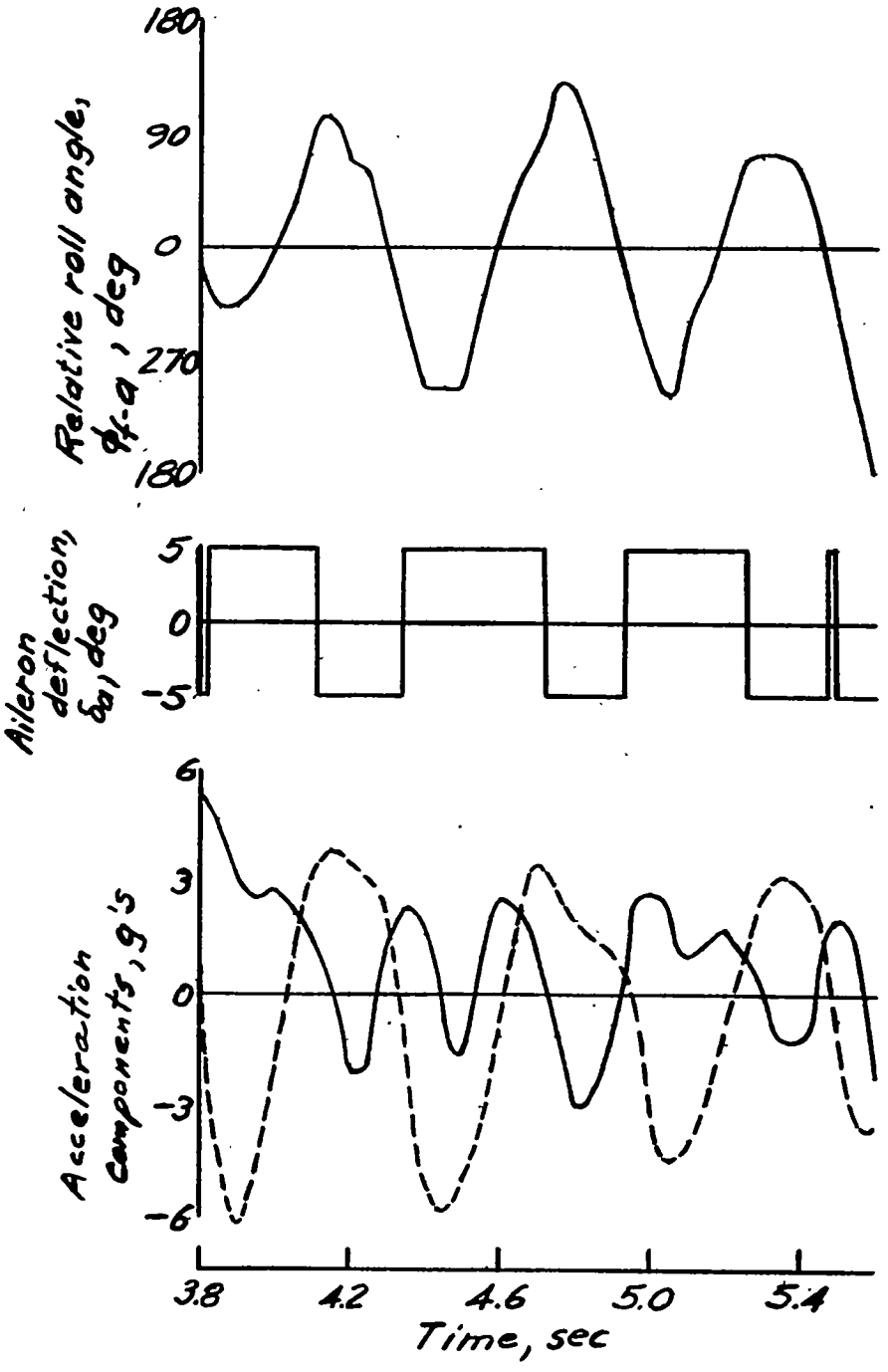

Figure 18.- Flight test data obtained as seeker hunted on target flare. Acquisition range, 1,250 feet. Mach number 1.24 to 1.0.

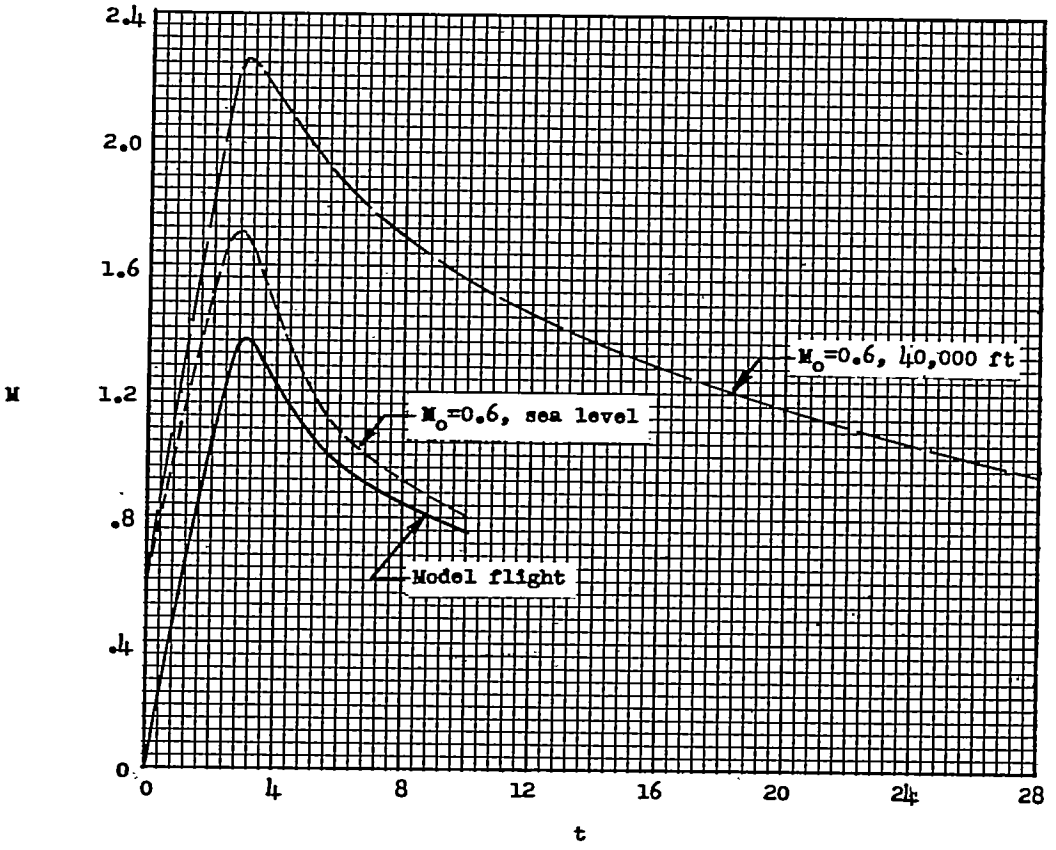

Figure 19.- Mach number time histories.

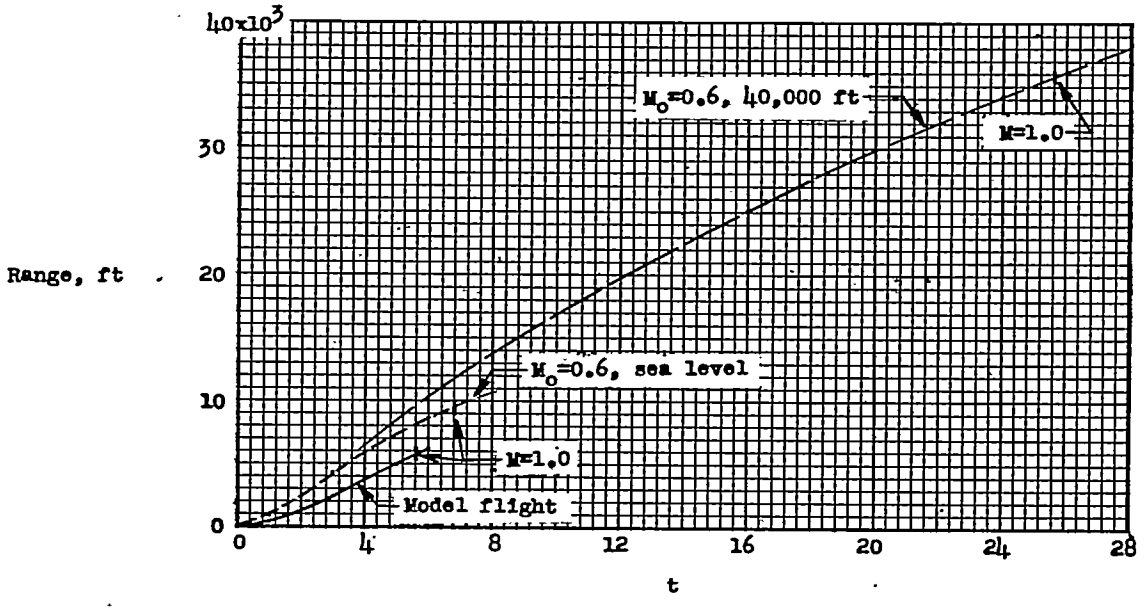

Figure 20.- Time histories of range from launching point.

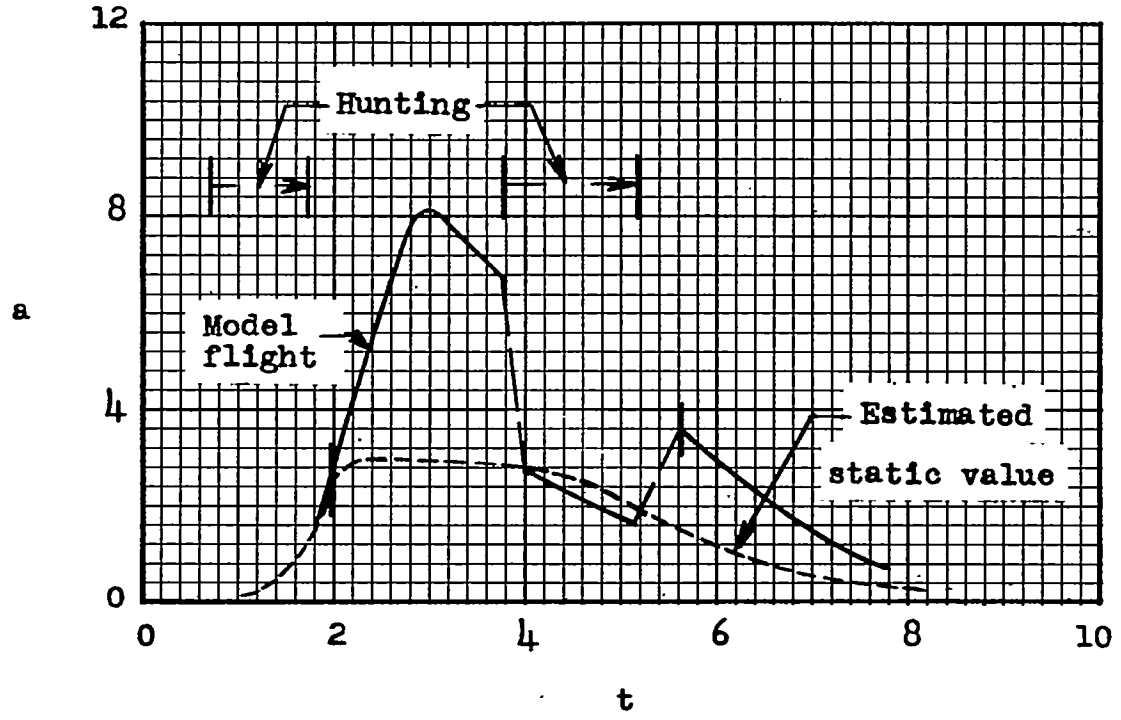

Figure 21.- Normal acceleration time histories.

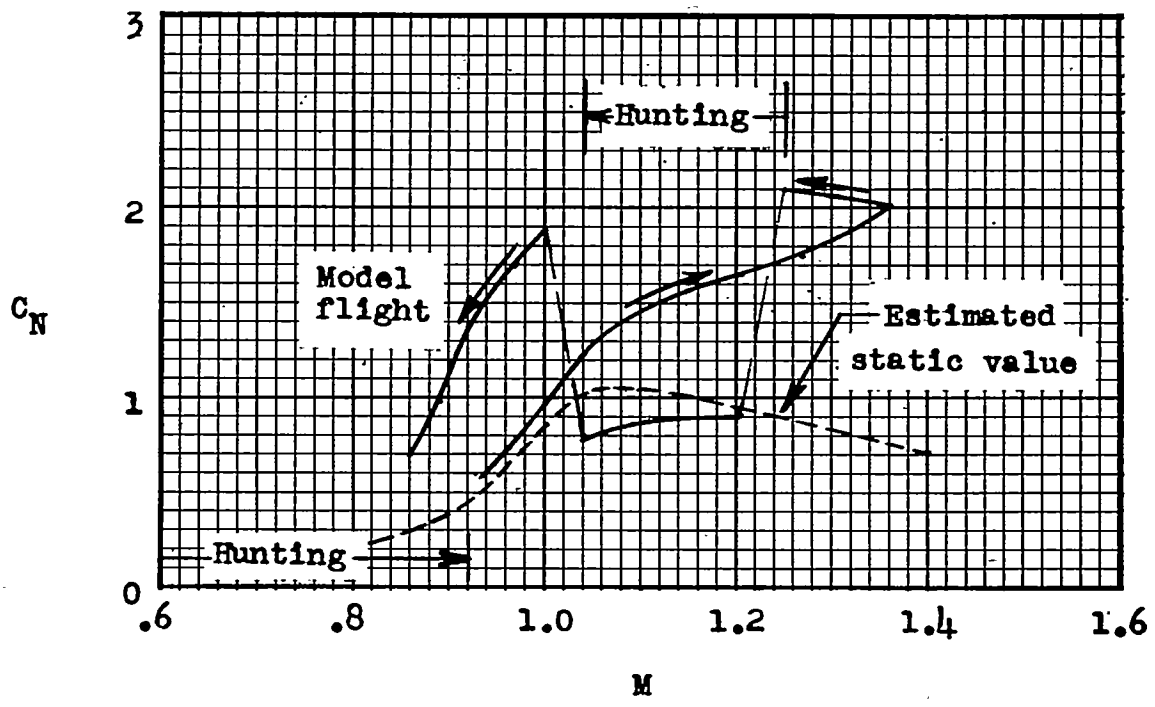

Figure 22.- Measured and estimated normal-force coefficients.

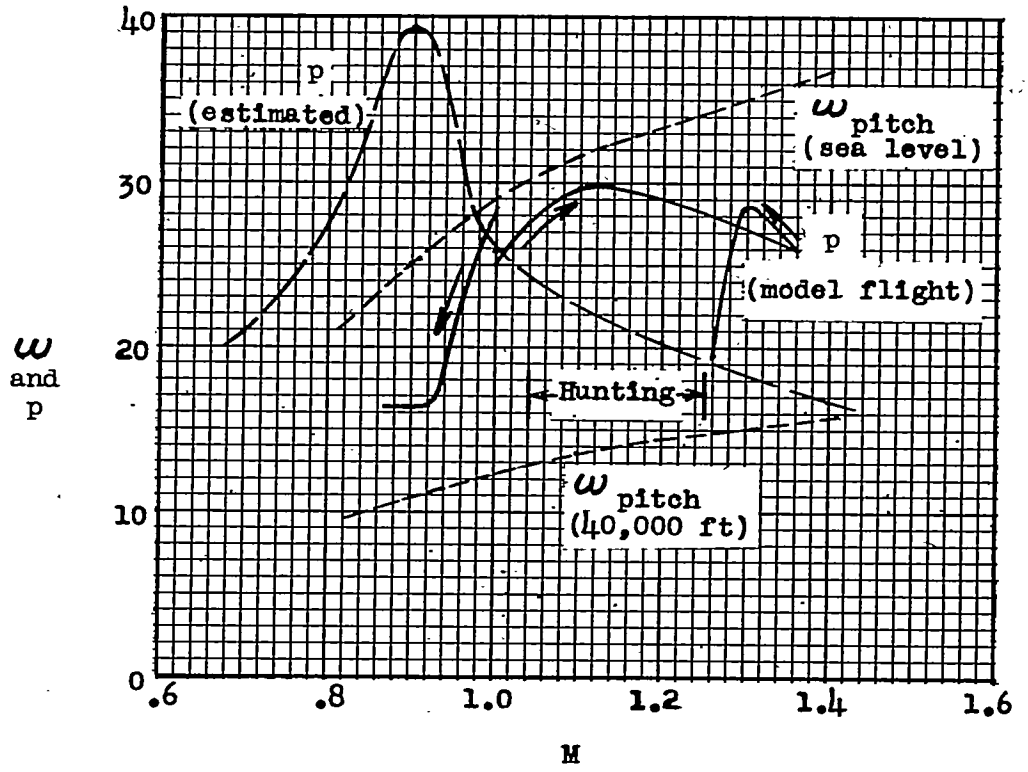

Figure 23.- Roll and pitch frequencies.

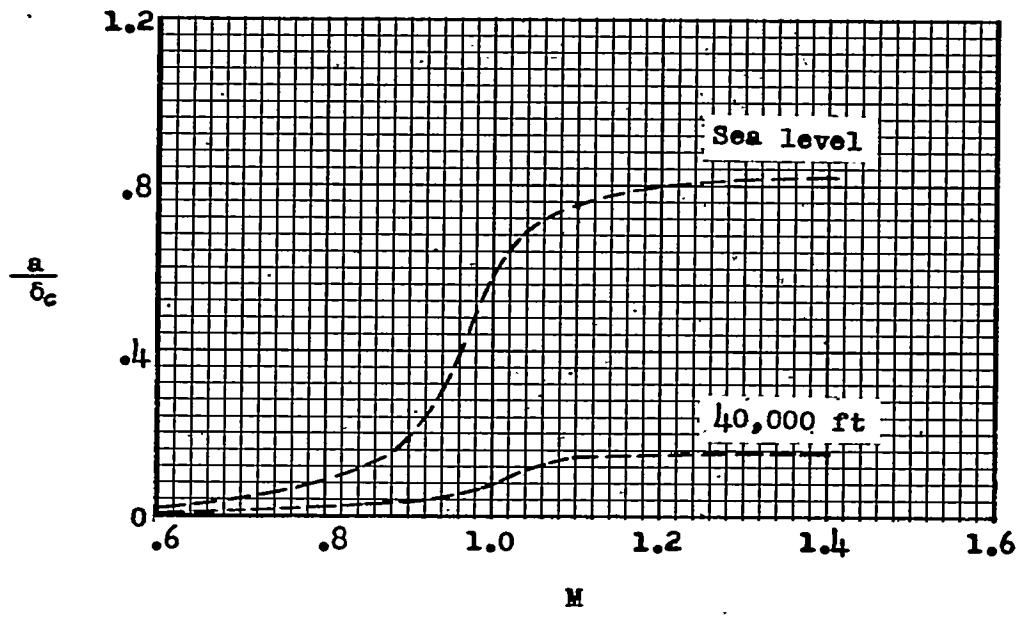

Figure 24.- Effect of altitude on maneuverability.

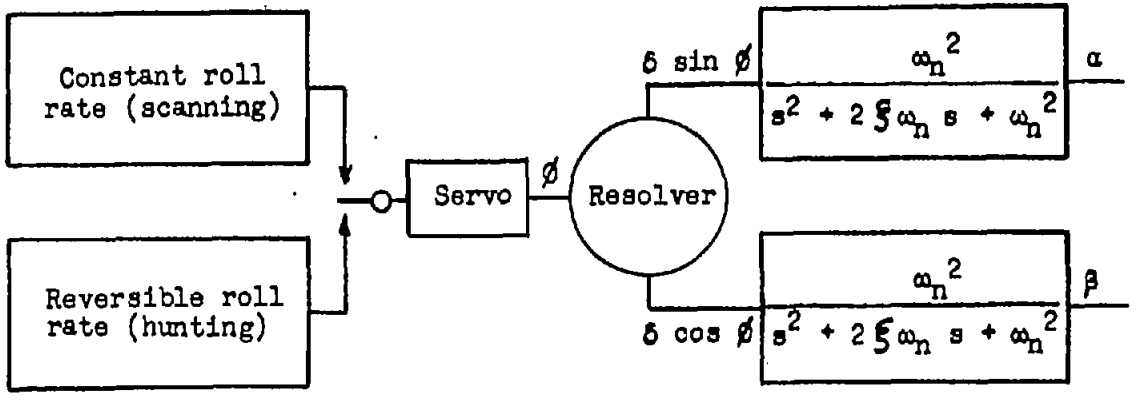

Figure 25.- Block diagram of analog simulation of rolling lift vector and airframe pitch and yaw short period mode of oscillation. $\xi = 0.1$.

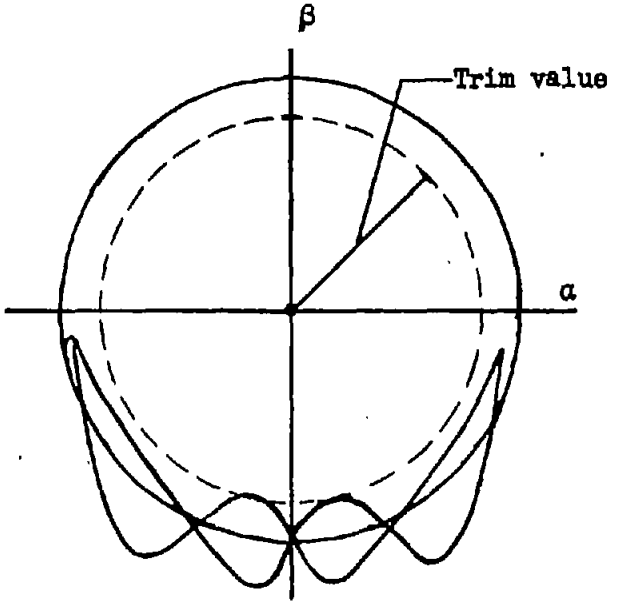

Figure 26.- Descriptive figure illustrating analog computer results. Solid curve is time locus of resultant angle of attack $\left|\sqrt{\alpha^2 + \beta^2}\right|$ during steady rolling and hunting. Dotted circle is time locus of trim value forcing function.

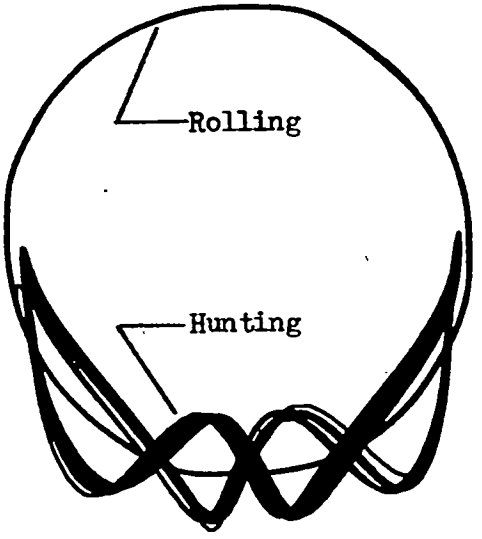

(a) Transition from rolling to hunting.

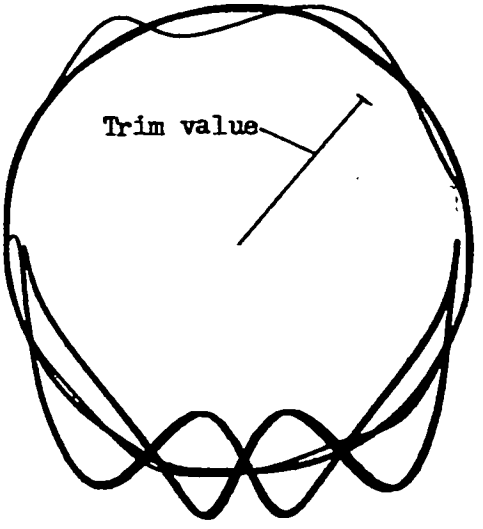

(b) Transition from hunting to rolling.

Figure 27.- Analog computer results showing time locus of resultant angle of attack. Ratio of rolling frequency to airframe frequency, 0.13. Hunt amplitude, $\pm 60^{\circ}$.

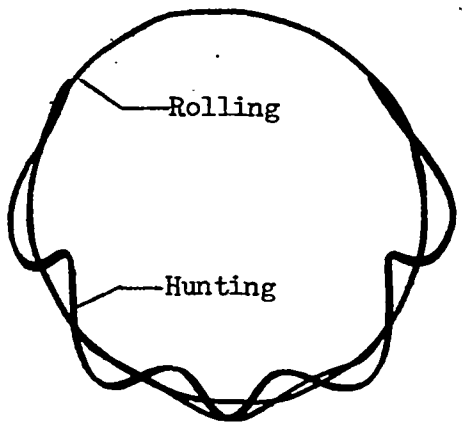

(a) Transition from rolling to hunting.

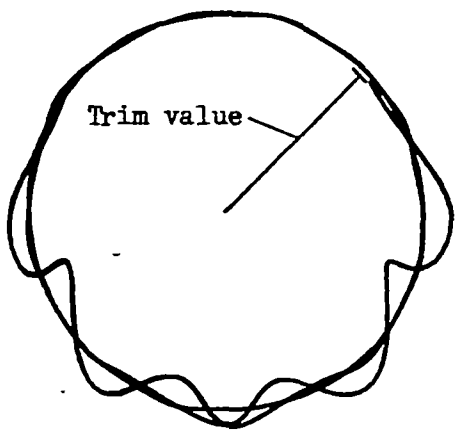

(b) Transition from hunting to rolling.

Figure 28.- Analog computer results showing time locus of resultant angle of attack. Ratio of rolling frequency to airframe frequency, 0.1. Hunt amplitude, $\pm 120^{\circ}$.

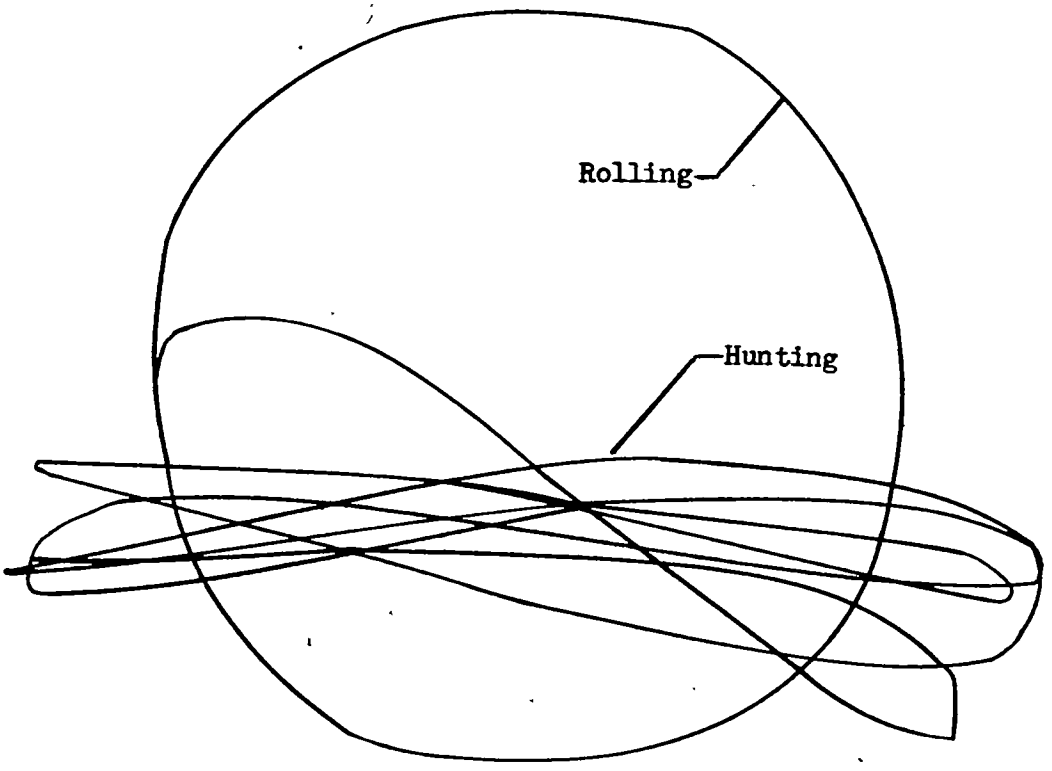

(a) Transition from rolling to hunting.

Figure 29.- Analog computer results showing time locus of resultant angle of attack. Ratio of rolling frequency to airframe frequency, 0.64. Hunt amplitude, $\pm 60^{\circ}$.

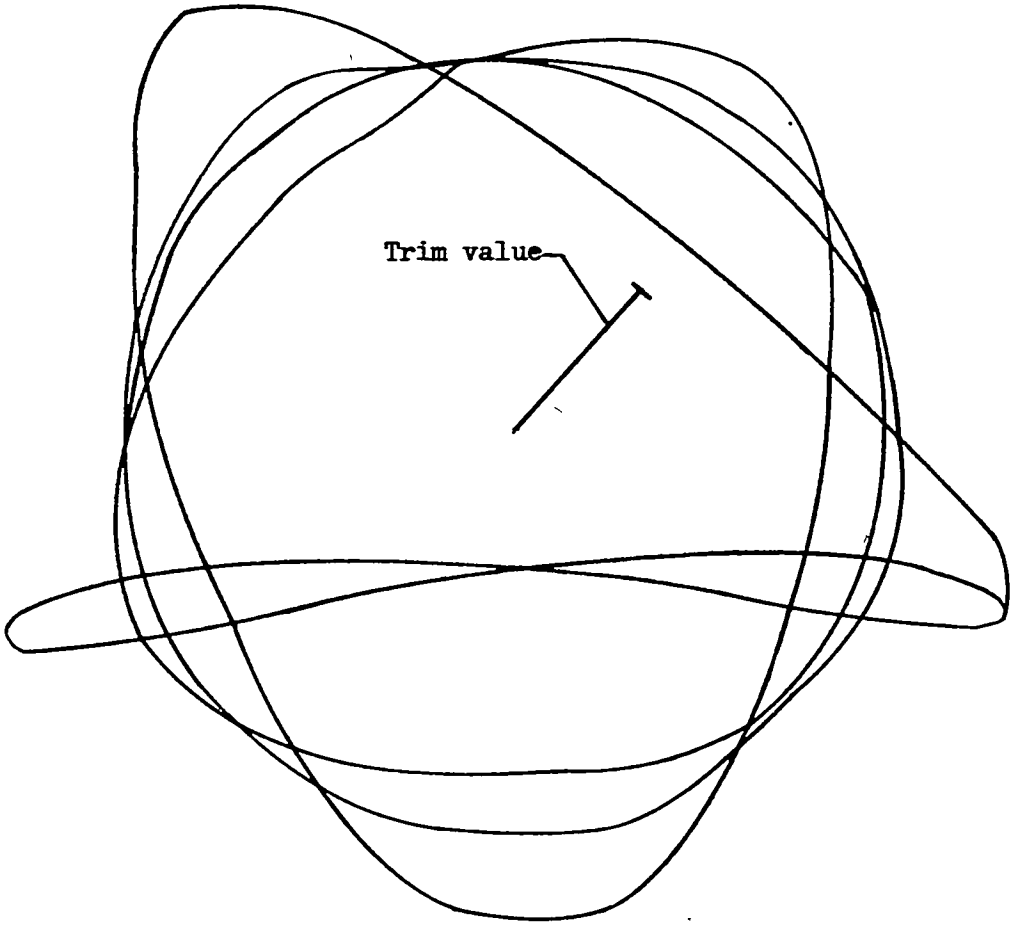

(b) Transition from hunting to rolling.

Figure 29.- Concluded.

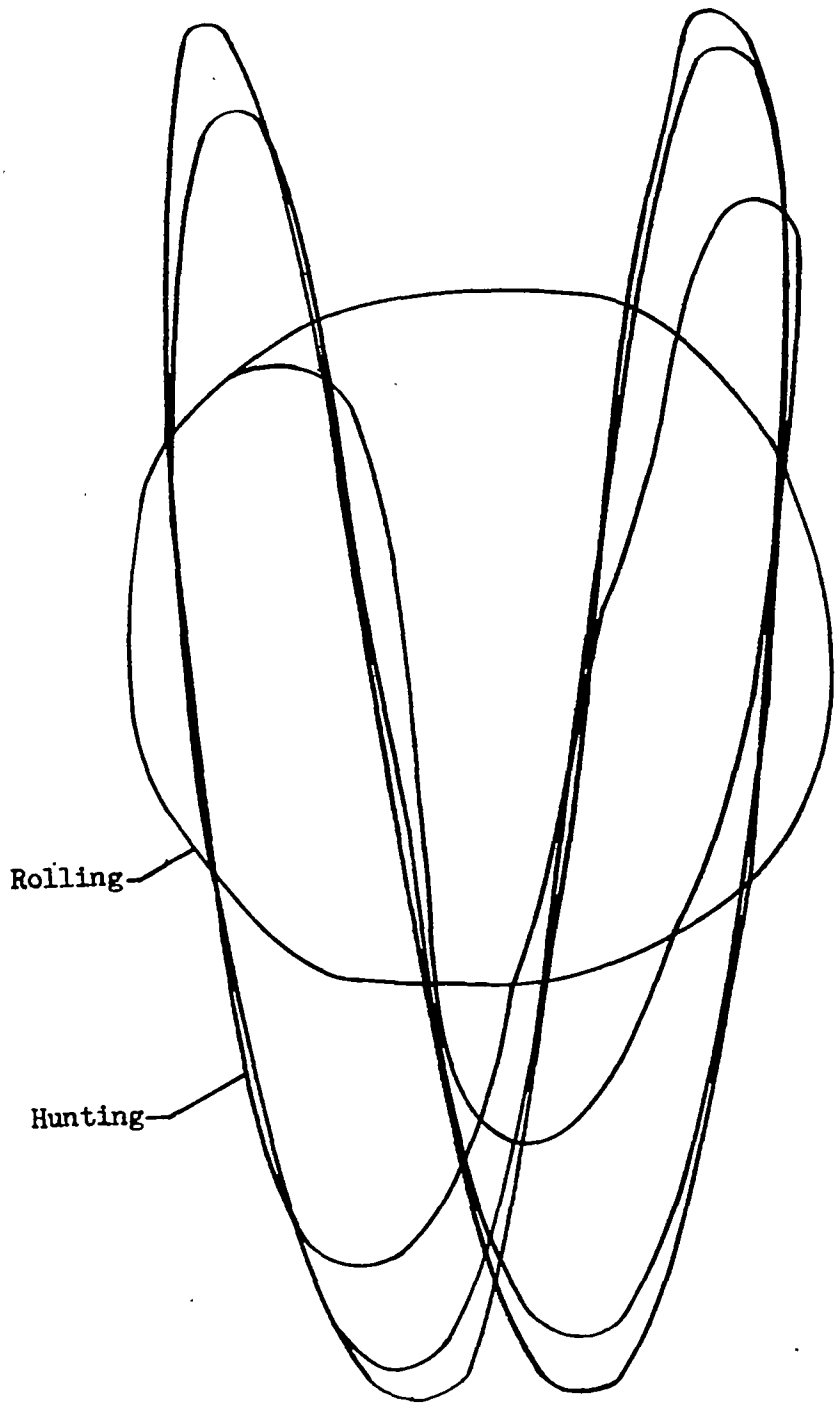

(a) Transition from rolling to hunting.

Figure 30.- Analog computer results showing time locus of resultant angle of attack. Ratio of rolling frequency to airframe frequency, 0.64. Hunt amplitude, ±120°.

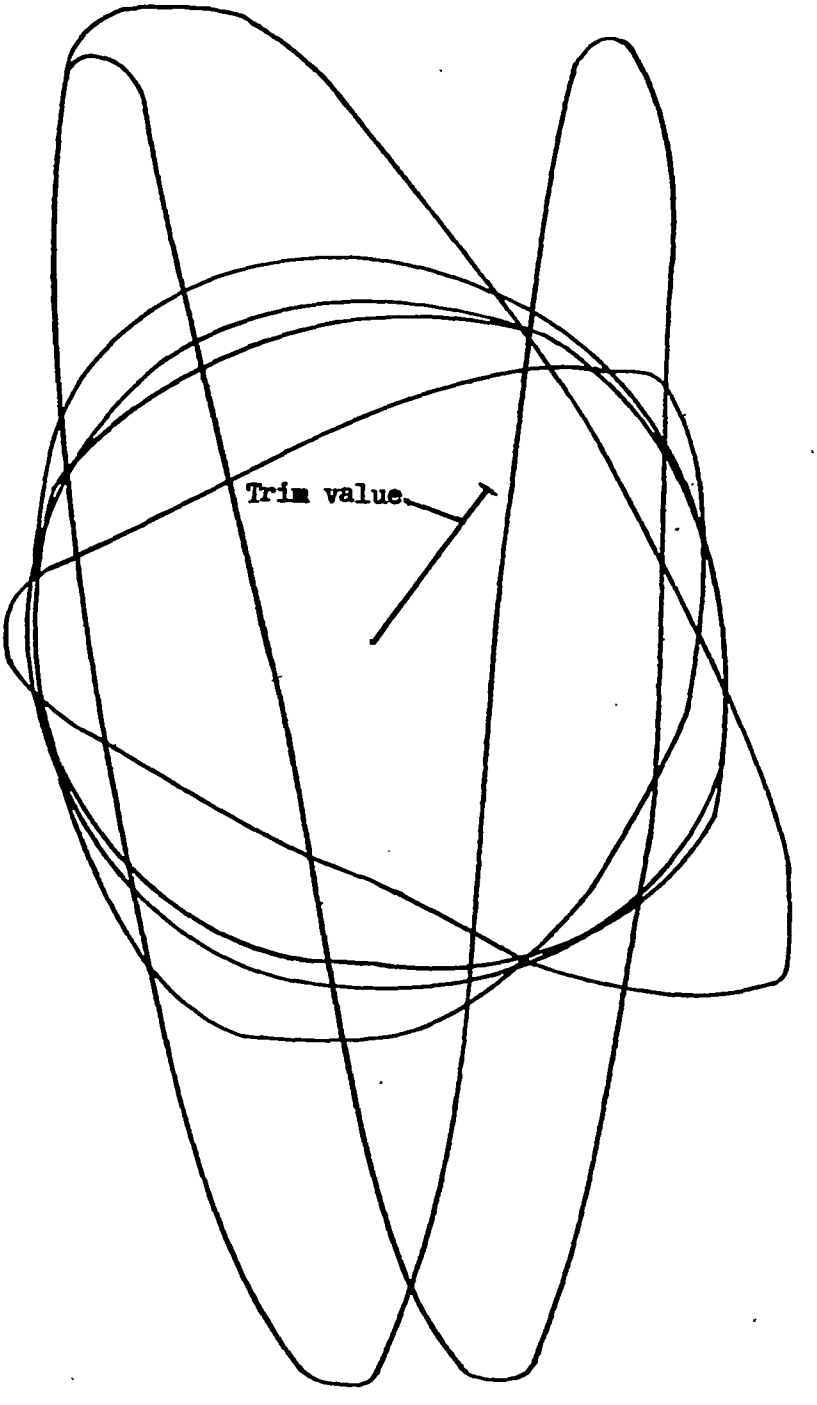

(b) Transition from hunting to rolling.

Figure 30.- Concluded.

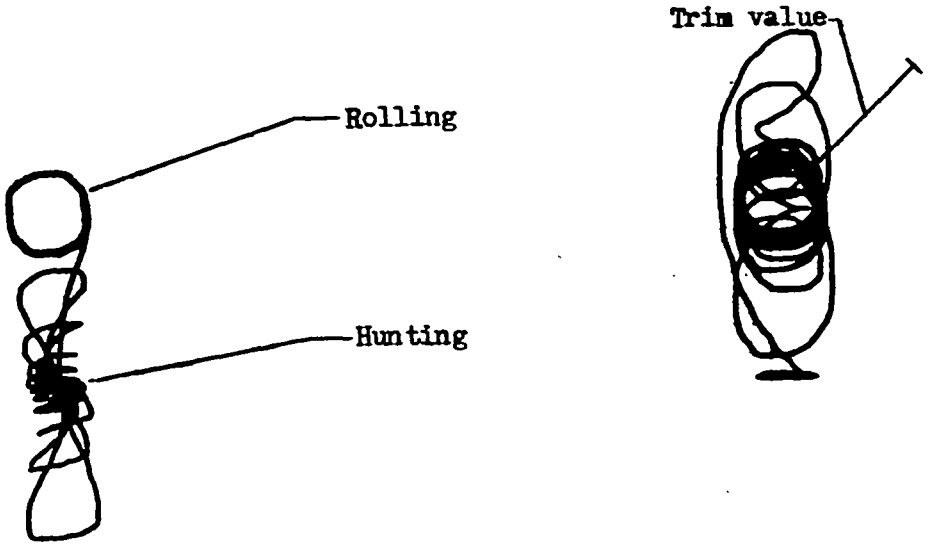

(a) Transition from rolling to hunting.

(b) Transition from hunting to rolling.

Figure 31.- Analog computer results showing time locus of resultant angle of attack. Ratio of rolling frequency to airframe frequency, 2.6. Hunt amplitude, ±60°.

(a) Transition from rolling to hunting.

(b) Transition from hunting to rolling.

Figure 32.- Analog computer results showing time locus of resultant angle of attack. Ratio of rolling frequency to airframe frequency, 2.6. Hunt amplitude, ±120°.

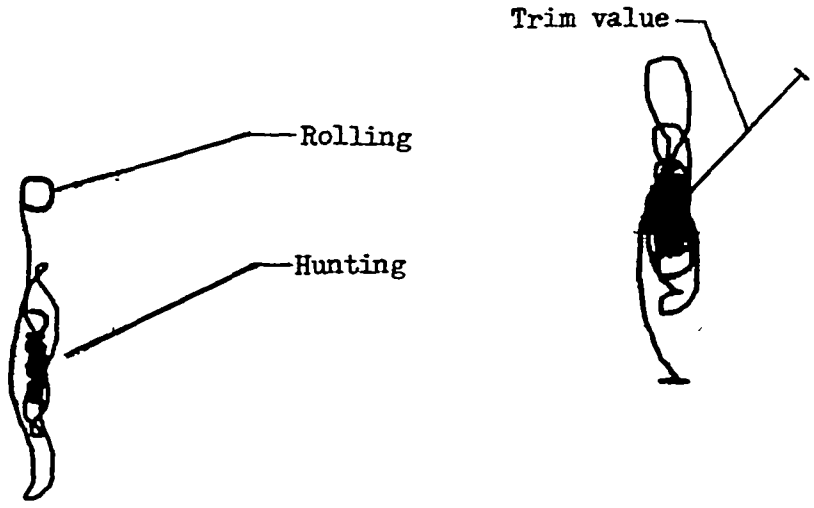

(a) Transition from rolling to hunting.

(b) Transition from hunting to rolling.

Figure 33.- Analog computer results showing time locus of resultant angle of attack. Ratio of rolling frequency to airframe frequency, 3.8. Hunt amplitude, $\pm 60^{\circ}$.

(a) Transition from rolling to hunting.

(b) Transition from hunting to rolling.

Figure 34.- Analog computer results showing time locus of resultant angle of attack. Ratio of rolling frequency to airframe frequency, 3.8. Hunt amplitude, $\pm 120^{\circ}$.

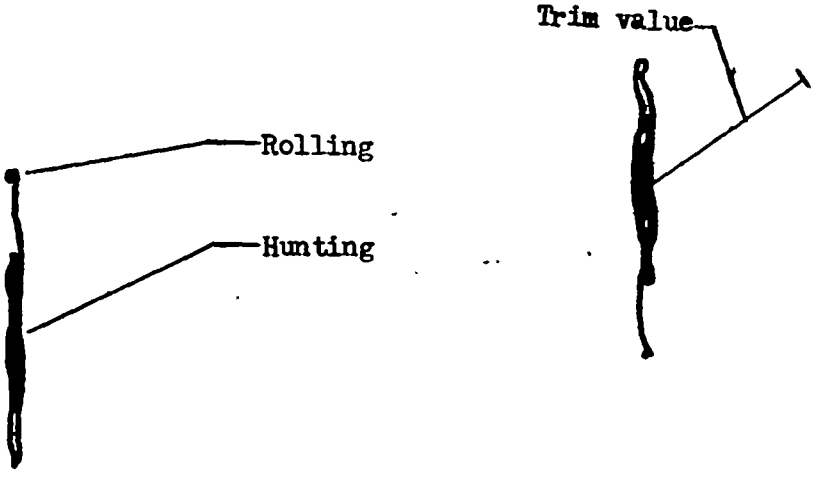

(a) Transition from rolling to hunting.

(b) Transition from hunting to rolling.

Figure 35.- Analog computer results showing time locus of resultant angle of attack. Ratio of rolling frequency to airframe frequency, 6.4. Hunt amplitude, ±60°.

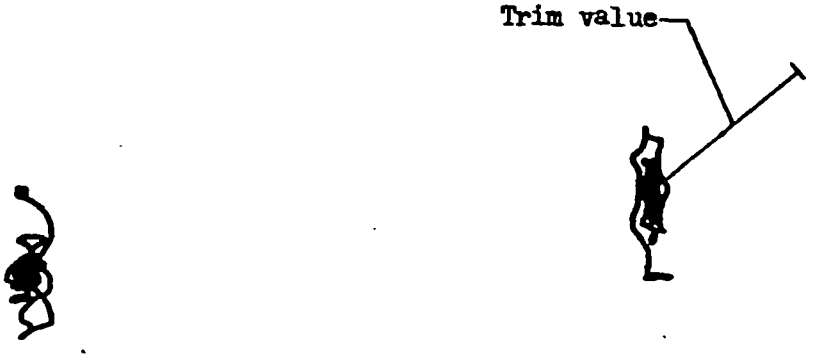

(a) Transition from rolling to hunting.

(b) Transition from hunting to rolling.

Figure 36.- Analog computer results showing time locus of resultant angle of attack. Ratio of rolling frequency to airframe frequency, 6.4. Hunt amplitude, ±120°.

NACA - Langley Field, Va.